PETROLOGY, GEOCHEMISTRY AND ORIGIN
OF THE SIERRA DE BAZA OPHIOLITES (BETIC CORDILLERA, SPAIN)

J.A Lozano Rodríguez*, Encarnacion Puga*, Claudio Natali**,✉, Gianluca Bianchini***,✉ and **Luigi Beccaluva*****

* *Instituto Andaluz de Ciencias de la Tierra (CSIC-UGR), Armilla, Granada, Spain*.
** *Dipartimento di Scienze della Terra, Università di Firenze, Italy*.
*** *Dipartimento di Fisica e Scienze della Terra, Università di Ferrara, Italy*.
✉ *Corresponding authors, e-mail: claudio.natali@unifi.it; bncglc@unife.it*

ABSTRACT

In this work we present for the first time a petrological-geochemical and genetic study of the Sierra de Baza ophiolites, which represent one of the ophiolitic occurrences of the Betic Cordillera (Southern Spain). They are composed of ultramafic, mafic and sedimentary rocks, largely affected both by ocean floor and polyphasic metamorphism during the Alpine orogeny. Ultramafic rocks are serpentinized lherzolites and harzburgites, whereas the metabasites are meta-gabbros and meta-basalts. On the whole, Sierra de Baza ophiolites show striking geochemical similarities with those from other Betic occurrences, as well as with other Tethyan ophiolites of the Western Mediterranean (Calabria, Internal and External Ligurides, Platta, Corsica and Western Alps). In particular, metabasites show petrological and geochemical features similar to the E-MORB magmatism of the Atlantic Ridge between 45 and 63ºN generated under ultra-slow spreading ridge conditions. This process originated a strip of few hundreds km of ocean floor at the western end of the Tethys, located SE of the Iberian-European margin during the Mesozoic. The inversion of the stress regime in the European-Iberian and African geodynamics, starting from the Late-Middle Cretaceous, caused subduction and metamorphism in the eclogite facies of oceanic slices that were partially exhumed on the continental margin, forming the Betic Ophiolites. These ophiolites were disarticulated and dismembered as a result of the shift towards SW of the Alboran continental block, progressively separated from the AlKaPeCa (Alboran, Kabilias, Peloritani, Calabria) microplate, finally occupying their current position in the Betic Internal Zones.

INTRODUCTION

The ophiolites of the peri-Mediterranean Alpine domain, reflect a complex geological history including oceanic spreading, subduction, collision and final obduction. These Alpine ophiolites plausibly represent remnants of several oceanic strands of Mesozoic age forming the Tethys Ocean and developed between the continental margins of the European and African plates, an area characterized by the presence of several microplates and/or continental blocks (Handy et al., 2010). These ancient oceanic domains are currently incorporated into the Alpine-Himalayan orogenic belts, as result of several subduction and continental collision events between the main Eurasian, African and Indian plates and a series of microplates (including the Iberian Plate) originated from Gondwana fragmentation throughout the Mesozoic (Zheng, 2012). In this framework, the ultramafic and mafic rocks included in the Betic Cordillera (SE Spain) have been interpreted as an ophiolite association, i.e., metamorphosed remnants of a Mesozoic oceanic lithosphere, since the 1970s (Puga, 1977; Puga and Díaz de Federico, 1978). This hypothesis relating the Betic Ophiolite Association (hereafter named as BOA following Puga,1990) to a Mesozoic oceanic basin, was criticized at the beginning, due to the paucity of outcrops conforming to the three layers defined for Ophiolites in the Penrose Conference (1972), i.e., sections including peridotites/serpentinites, gabbros/basalts and deep sea sediments, such cherts, hypothetically corresponding to the stratigraphy of the oceanic lithosphere. In spite of this criticism, the Betic Ophiolites were identified as Mid-Oceanic-Ridge (MOR)-type by Puga (1977;1990), Bodinier et al. (1988), Morten et al. (1987), Puga et al. (1989a;1989b), who investigating BOA mafic and ultramafic lithologies emphasizing geochemical analogies with the rocks formed along the Atlantic Ridge and those included within the Jurassic Alpine-Apennine ophiolites. Later palaeogeographic, petrologic and geochemical studies (Guerrera et al., 1993; Puga et al., 1995; 1999b; 2000) corroborated the ophiolitic origin of the BOA rocks. Nevertheless, Gómez-Pugnaire et al. (2000) highlighted apparent petrological incongruence, emphasizing that the geochemical composition of Betic basalts/gabbros do not conform to Normal Mid Oceanic Ridge Basalt (N-MORB) and that the Betic ultramafic rocks are less residual with respect to the abyssal peridotites having prevalent harzburgite composition. This criticism on the oceanic nature of the BOA has been largely bypassed by recent papers which coupled geochronological data with new petrological and geochemical studies (e.g., Ruiz Cruz et al., 1999; 2007; Puga et al., 2002a; 2002b; 2005; 2007; 2009; 2011; Alt et al., 2012; Aerden et al., 2013), certainly ascribing the provenance of some BOA outcrops to a MORB-type tectonic setting, or to an Ocean-Continent-Setting (OCT). This hypothesis conforms to the interpretations proposed for ophiolite sequences of the Alps and Apennines (Beccaluva et al., 1979; Rampone et al., 1995; 2005; 2008; 2009; 2014; Marroni et al., 1998; Rampone and Piccardo, 2000; Borghini et al., 2007; 2016; Montanini et al., 2008; Manatschal and Müntener, 2009; Piccardo and Guarnieri, 2010; Rampone and Hofmann, 2012; Lagabrielle et al., 2015; Saccani, 2015). Worth of note, recent oceanographic studies emphasize that the rock associations of modern oceanic floors are more heterogeneous than what assumed in the past (e.g., Dick et al., 2003; Gale et al., 2013; Herbrich et al., 2015; Regelous et al., 2016) and, hence, the "ophiolite concept" interpreted as "fossil oceanic lithosphere with a unique and complete lithologic sequence" has also to be revisited and updated (Lagabrielle, 2009).

44

In this work, 55 meta-mafic and 17 meta-ultramafic rock samples collected from Sierra de Baza have been analyzed for their major trace element composition, and Sr-Nd isotopes were analyzed on 8 selected samples, in order to highlight analogies and differences with the other BOA sequences, with the final aim of better understanding the BOA in the framework of the Mesozoic Tethys puzzle, within the paleogeographic and geodynamic evolution of the Central-Western Mediterranean area.

GEOGRAPHICAL AND GEOLOGICAL SETTING OF THE SIERRA DE BAZA OPHIOLITES

The Betic Ophiolites Association (BOA), crops out discontinuously along 250 km in the central and eastern sectors of the Betic Cordillera (SE Spain, Supplementary Fig. 1). The BOA rocks are represented by tectonic slices ranging in size from decametres to kilometres, made by metamorphosed ultramafic and mafic lithologies sometimes associated with sedimentary rocks. These ophiolites are exclusively located in the Mulhacén Complex (MC), in the central and
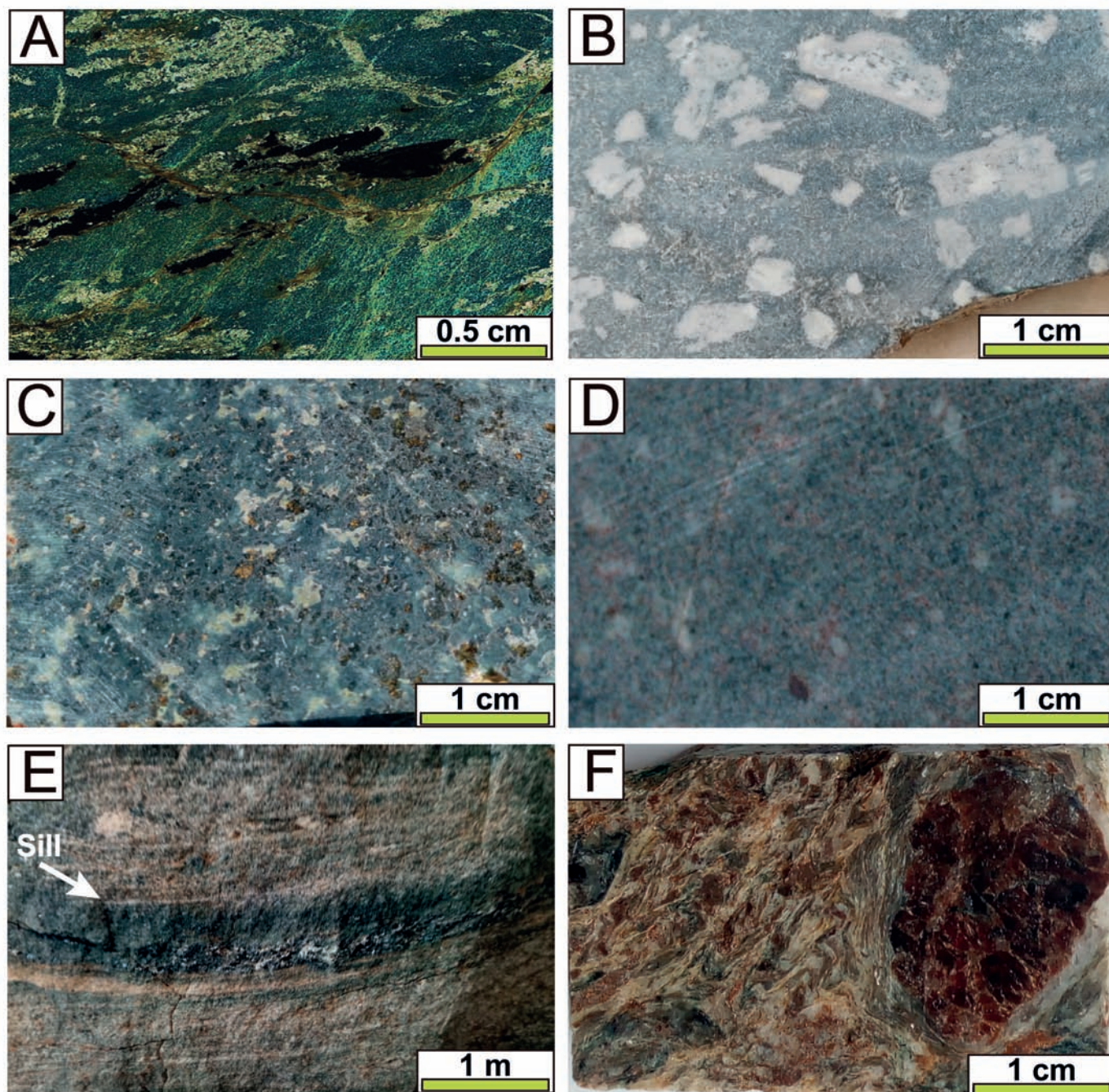

Fig. 1 - Macroscopic appearance of some BOA rocks in Sierra de Baza. A: serpentinite from a secondary harzburgite (Cani-277), showing large Magnetite crystals, surrounded by serpentinite (antigorite), along with minor chlorite and talc; B: Amphibolite from a porphyry textured gabbro, showing white phenocrysts of plagioclase in a doleritic matrix (Cani-83); C: Eclogite from pyroxene-rich gabbro (Cani-139B); D: Eclogite from basalt (CH-37); E: Epidote amphibolite from dolerite (sill) intruded into micaschists (Cani-285); F: Micaschists with large garnet porphyroblasts from a metapelite of the sedimentary sequence (Cani-252).

eastern area of the Betic Cordillera, and are never found in the underlying Veleta Complex (VC, Puga et al., 2002a; 2004a; 2004b; 2007; Aerden et al., 2013). This suggests that these two complexes pertained to different paleogeographic domains before and during the Jurassic-Cretaceous period, when the ophiolites originated from exhumation of an oceanic floor (Guerrera et al., 1993; Tendero et al., 1993; Puga et al., 1999a; 1999b; 2005; 2009; 2011). The VC rocks crop out through several tectonic windows below the (MC), forming the Nevado-Filábride Domain and representing the deepest rocks in the current tectonic pile of the Betic Cordilleras (Figs. 1A, 1B). The BOA outcrops, deriving from the Betic oceanic floor (Guerrera et al., 1993; Puga et al., 2002a; 2011), allow the reconstruction of the pristine oceanic lithostratigraphy represented in Supplementary Fig. 1. Parts of the oceanic floor were obducted on the crustal rocks (Caldera unit of the MC) of its adjoining western continental margin, and overthrust by those from its eastern continental margin (Sabinas crustal unit).

Each of these continental units consists of rocks deriving from a Paleozoic basement with abundant granitic and rhyolitic orthogneisses, covered by Triassic sediments (Nieto, 1996; Nieto et al., 2000; Puga et al., 2002a; 2004b; 2007). The main rock types forming the ophiolite unit in the lithostratigraphic reconstruction are, from bottom to top: serpentinites, intruded by rodingitized dolerite dykes, and eclogitized/amphibolitized gabbros, dolerite dykes and basalts. These rock types may be found covered by a metasedimentary sequence in which the intercalation of amphibolitized dolerite sills is common, probably deriving from thin basaltic levels. Among the BOA, those from Sierra de Baza are characterized by the largest number of outcrops and by a notable linear extension of about 23 km, from the town of Charches to the west, to the Los Olmos locality to the northeast. (Supplementary Fig. 1C). In particular, the size of the ultramafic bodies in Sierra de Baza ranges from 6-7 m in Las Canteras (2.5 km southeast of Los Olmos) to about 700 m in the outcrop known as La Canaleja.

SAMPLES AND ANALYTICAL METHODS

72 rock samples were collected from the Sierra the Baza complex. The Sierra de Baza mafic rocks (55 samples) consist of metamorphosed (olivine)-gabbros, dolerites and basalts. The meta-ultramafic rocks (17 samples) of the Sierra de Baza mainly consist of partially serpentinized lherzolites and harzburgites. Major element and Zr concentrations were determined on glass beads made of 0.6 g of powdered sample diluted in 6 g of $Li_2B_4O_7$ using a PHILIPS Magix Pro (PW-2440) X-ray fluorescence (XRF) spectrometer at the "Centro de Instrumentación Científica" of Granada University (40 samples). Precision was better than ±1.5% for a concentration of 10 wt%. Precision for Zr was better than ±4% at a concentration of 100 ppm. Trace elements other than Zr were determined at the University of Granada by ICP-mass spectrometry (ICP-MS) using a PERKIN ELMER Sciex-Elan 5000 spectrometer; sample solutions were prepared by digesting 0.1 g of sample powder with HNO_3 + HF in a Teflon-lined vessel at ∼ 180°C and ∼ 200 p.s.i. for 30 min, subsequently evaporated to dryness and dissolved in 100ml of 4 vol% HNO_3. The concentrations of the PM-S and WS-E international standards were not significantly different from the recommended values (Govindaraju, 1994). Precision was better than ±5% and ±2% for concentrations

of 5 and 50 ppm, respectively. Sr-Nd isotope analyses were carried out at the University of Granada, where whole-rock samples were digested as described for the ICP-MS analysis, using ultra-clean reagents, and analyzed by thermal ionization mass spectrometry (TIMS) using a Finnigan Mat 262 spectrometer after chromatographic separation with ion exchange resins. Normalisation values were $^{86}Sr/^{88}Sr = 0.1194$ and $^{146}Nd/^{144}Nd = 0.7219$. Blanks were 0.6 and 0.09 ng for Sr and Nd respectively. External precision (2σ), estimated by analyzing 10 replicates of standard WS-E (Govindaraju, 1994), was better than 0.03% for $^{87}Sr/^{86}Sr$ and 0.015% for $^{143}Nd/^{144}Nd$. The measured $^{87}Sr/^{86}Sr$ of the NBS 987 international standard was 0.710250±0.000044, whereas measurements of the La Jolla Nd international standard yielded a $^{143}Nd/^{144}Nd$ ratio of 0.511844±0.000065.

PETROGRAPHY

Meta-ultramafic and meta-mafic rocks have been studied under polarized light optical microscope. The petrographic and mineralogical features, together with sample location, are reported in Tables 1 and 2. The lithologies forming the BOA in Sierra de Baza are the following: a) serpentinized lherzolites where relics of diopsidic clinopyroxene and spinel are preserved and serpentinized harzburgites in which acicular aggregates of olivine and orthopyroxene can be recognized (Fig. 1A); b) gabbros, crossed by dolerite dikes, mostly metamorphosed in eclogites and/or amphibolites, sometimes preserving plutonic or hypabyssal structures (Fig. 1B, C and D); c) basalts, which sometimes preserve flow structures and padded forms (pillow lavas, Fig. 1D); d) micaschists (Fig. 1E and F) and micaceous quartzites, with transition to calcschists with ankerite nodules, which are more abundant in the upper part. The gabbros, basalts and sedimentary lithologies in Sierra de Baza are similar to the lithologies from other outcrops of the BOA previously described by Puga et al. (2017). As mentioned above, meta-ultramafic rocks are mostly serpentinites sometimes preserving clinopyroxene relics characterized by chemical composition similar to that of fertile spinel lherzolites. The primary mineral association was constituted by olivine, clinopyroxene (diopside), orthopyroxene (enstatite), chromium-spinel, replaced by antigorite, chromium-magnetite and chlorite, talc and minor tremolite-actinolite. The antigorite matrix, which often surrounds the porphyroblasts of the other metamorphic minerals, is probably derived from olivine crystals. Chromium chlorite and chromium magnetite aggregates (Fig. 2A-1 and A-2), which probably replaced pre-existing chromium spinel, together with diopside and tremolite, were formed in successive, high and medium pressure metamorphic events. Clinohumite can also be observed (Lopez Sanchez-Vizcaıno et al., 2005). Serpentinized lherzolites generally contain antigorite, penninite, chromium and aluminium magnetite, diopsidic-clinopyroxene, titano-clinohumite and olivine (Fig. 2A-1). Serpentinized harzburgites generally contain antigorite, penninite, chromium magnetite and aluminum magnetite, talc, clinochlore and relics of olivine and orthopyroxene (Fig. 2A-2).

Meta-mafic rocks are abundant in Sierra de Baza, especially in the western sector, and are mainly eclogites and amphibolites derived from gabbros and dolerites. Samples preserved porphyric, gabbroid or doleritic igneous structures, mainly constituted by intergrowth of plagioclase and pyroxene crystals of different sizes, together with olivine
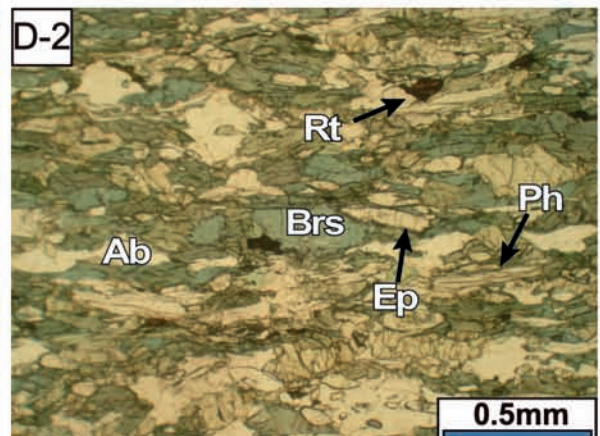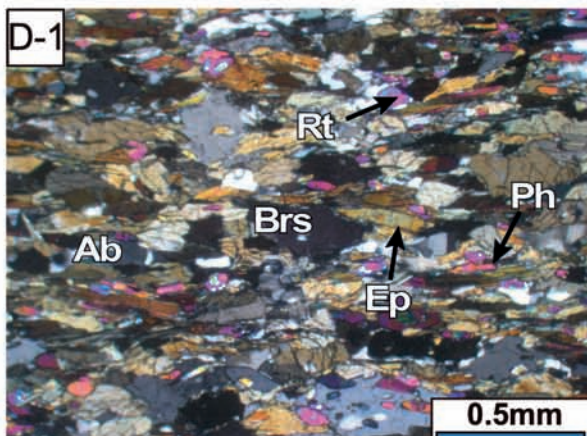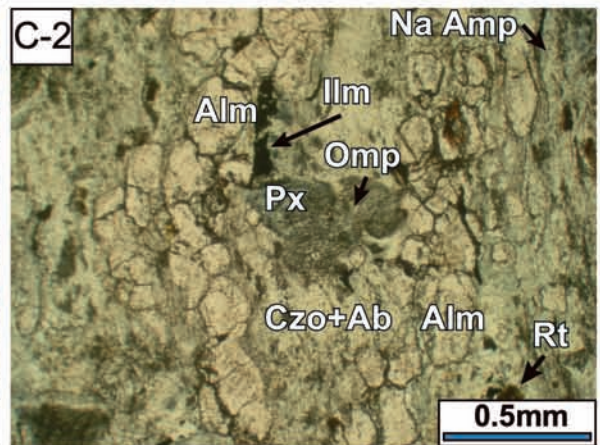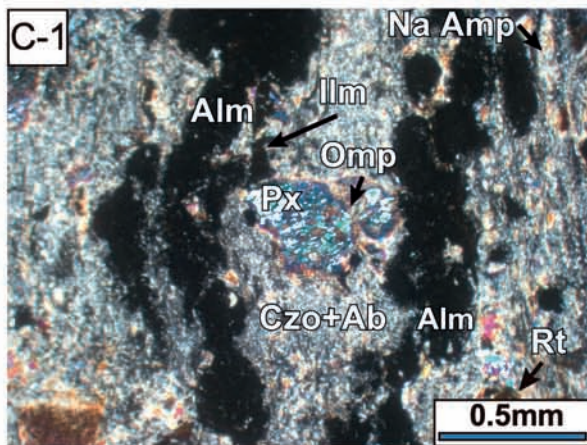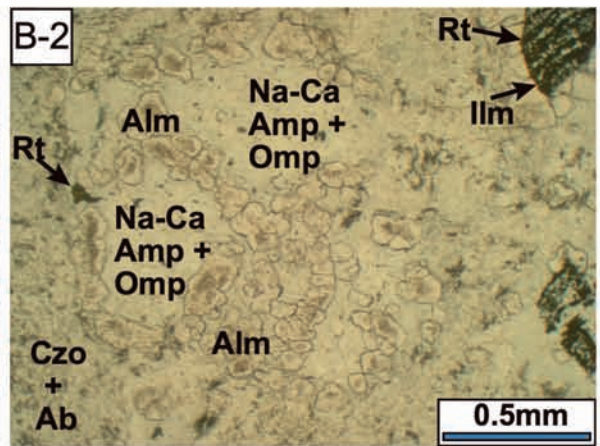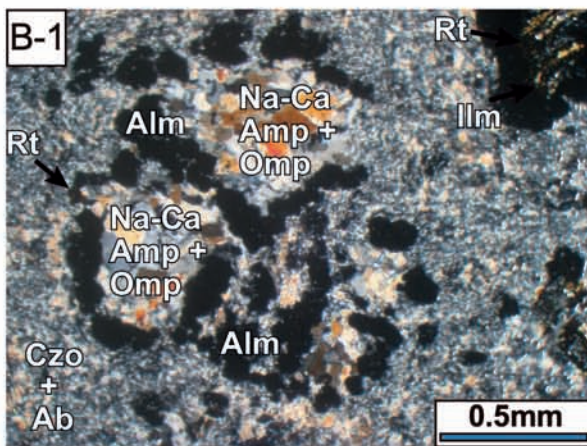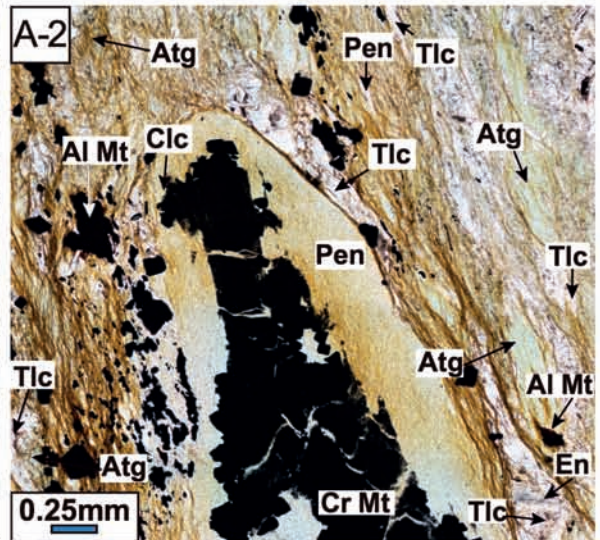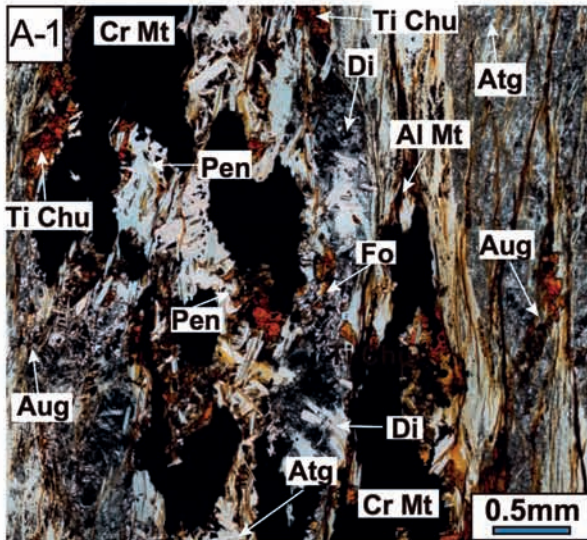
(Fig. 1B, C and D). The minerals that constitute igneous paragenesis have been scarcely preserved in studied samples and can be identified only by microtextural analysis in some meta-basalts and meta-gabbros of the Cóbdar ophiolite, where relics of igneous parageneses formed by plagioclase, olivine ± clinopyroxene (augite) and ilmenite are recognized (Puga et al., 1999a; 2000; Puga 2005). Many of the meta-mafic rocks from Sierra de Baza show a great mineralogical complexity developed by the superposition of different post-magmatic processes throughout their evolution. The eclog-ites with porphyroblastic texture show aggregates of large, variously oriented omphacitic pyroxene and, to a lesser extent, garnet crystals, in a matrix formed by albite and epi-dote microcrystal intergrowth resulting from the metamor-phic transformation of plagioclase. In the matrix of eclogites remnants of pristine ilmenite are found, together with more abundant rutile aggregates (Fig. 2B-1 and B-2). In many cases rutile crystals are present as small needles included in omphacite, indicating its formation during eclogitic meta-morphism from preexisting ilmenite. A common feature is the formation of hydrated minerals at the edges of ompha-cite and garnet, typical of amphibolite and green schists fa-cies parageneses, which partially superimposed the eoalpine eclogitic mineral assemblages during the subsequent me-soalpine and neoalpine episodes. These retrometamorphic minerals are fundamentally sodium-calcium amphibole and colorless mica (phengite). Crowns of almandine gar-net that surrounds polymorphic aggregates mainly formed by omphacite and amphibole, are generally surrounded by aggregates of fine-grained albite and clinozoisite (Fig. 2B-1 and B-2), and amphibolitized eclogites also include symplectitic textures. Some of the meta-basalts derive from massive lavas mainly with columnar jointing and, to a lesser extent, pillow lavas and subvolcanic dikes. Meta-basalts usually preserve variolitic or porphyritic textures, although the primary igneous phenocrysts and the matrix have been completely replaced by metamorphic minerals during meta-morphism in the eclogitic or amphibolitic facies (Fig. 2C-1 and C-2). In spite of the metamorphic recrystallization, the typical tholeiitic crystallization sequence, in which olivine is followed by a plagioclase and clinopyroxene can still be envisaged. Augitic clinopyroxene is generally replaced by omphacite and rutile, whereas plagioclase is mainly trans-formed into an aggregate of clinozoisite and paragonite, and, to a lesser extent, in glaucophane, during eclogitic metamor-phism. The eclogitic mineral assemblage was affected by retrograde metamorphism in the Ab-Ep amphibolitic facies, forming albite, pistacite and various types of amphiboles, such as pargasite, edenite and tremolite, which formed at the expenses of the omphacite. The almandine shows edges characterized by symplectitic texture made of aggregates of Na-Ca amphibole crystals and phengite. Plagioclase is replaced by intergrowth of clinozoisite and albite (Fig. 2C-1

and C-2) or paragonite. Figs. 2D-1 and D-2 show an Ab-Ep amphibolite (Cani-26A) that presents an equilibrium mineral association of amphibole, epidote, albite, mica, chlorite and quartz. The mineral preferential orientation of metabasites, including the Na-Ca amphibole porphyroblasts forming a nematoblastic texture, follow the main foliation of the mi-cashist, suggesting a common metamorphic process.

RESULTS

Whole rock geochemistry

The Sierra de Baza meta-mafic rocks

The major and trace element, as well as Sr-Nd isotope composition of the meta-mafic rocks from the Sierra de Baza is reported in Tables 3, 4 and 5. The MgO content is quite variable for the different lithotypes, ranging from 4.53 to 10.14 (wt%) in the meta-(Fe)-gabbros, from 2.99 to 9.10 (wt%) in meta-(Fe)-dolerites and from 2.99 to 11.94 (wt%) in meta-basalts. The TiO_2 content ranges from 0.83 to 3.91 (wt%) in the meta-(Fe)-gabbros, from 0.99 to 3.24 (wt%) in meta-(Fe)-dolerites and from 1.13 to 2.49 (wt%) in meta-basalts. The LOI content is generally low, varying from 0 to 3.33 (wt%) in the meta-(Fe)-gabbros, from 0.77 to 3.77 (wt%) in meta-(Fe)-dolerites (with the exception one sample showing a maximum value of 5.07 wt%) and from 0.60 to 4.69 (wt%) in meta-basalts.

In the TAS (Total Alkali-Silica) classification diagram, meta-mafic rocks show subalkaline (basalt and andesitic basalt) to transitional and alkaline (basanite, basalt and trachybasalt) affinities (Fig. 3A). However, in the Nb/Y *vs* Ti/Zr binary diagram (Pearce, 1996), which is based on the ratios of less mobile element, more appropriate for the clas-sification of meta-mafic rocks, Sierra de Baza samples show a subalkaline affinity (Fig. 3B). This is also confirmed by the tholeiitic differentiation trend defined by these rocks on the ternary diagram of Irvine and Baragar (1971; Fig. 3C). In the Ti/1000 *vs* V tectonomagmatic diagram (Fig. 4A; Pearce, 2003) Sierra de Baza meta-mafic rocks show a typi-cal MORB affinity, similar to other Alpine ophiolites such as the Ligurides, those from Corsica, Gets, Platta (Bill et al., 2000; Desmurs et al., 2002; Saccani et al., 2008; Montanini et al., 2008), and to other BOA occurrences (Puga et al., 2017). The amphibolitized sample Cani-300 shows com-paratively higher Ti and V content probably deriving from a higher differentiation of the basaltic magma following the tholeiitic trend. On the other hand, samples Cani-288A and CH-12 plot outside of the MORB field in the Ti/1000 *vs* V diagram, showing a comparatively higher Ti/V ratio. The Sierra de Baza meta-mafic rocks have been also plot-ted in the Nb/Yb *vs* Th/Yb tectonomagmatic discrimination diagram of Pearce (1982), in which they mostly plot in the MORB-OIB mantle array, conforming to E-MORB-type

Fig. 2 - Plane polarized (right) and crossed-polarized (left) light photomicrographs of Sierra de Baza meta-mafic and meta-ultramafic rocks. A-1: Serpentinite (Cani-284) after lherzolite formed by diopside (Di) and forsteritic olivine (Fo) in a serpentine (Srp) matrix. It also shows aggregates of chromium magnetite (Cr Mt) altered to penninite (Pen) and Ti-clinohumite (Ti-Chu) coexisting with Fo, compatible with high P Eoalpine conditions; A-2: Serpentinite (Cani-277) after secondary harzburgite, with large Mt crystals, surrounded by Atp-type Srp, and minor chlorite (Chl) and talc (Tlc). Transformation of Cr Mt to Penninite (Pen) at the edge is observed. Enstatitic orthopyroxene (En) in a matrix formed by antigorite (Atg) and Tlc; B-1 and B-2: Eclogite after pyroxene-olivine gabbro, partially amphibolitized (CH-43) with coronitic texture where olivine has been replaced by omphacite (Omp) + almandine (Alm), the former subse-quently transformed into sodium-calcium amphibole (Na-Ca Amp); C-1 and C-2: Eclogite with fluidal texture, replaced by an aggregate of very fine-grained clinozoisite (Czo) and albite (Ab) after igneous plagioclase, alternated with Alm and Omp beds originated in the eclogitic facies (RA-33B); D-1 and D-2: Amphibole epidotite with transition to amphibolite (Cani-26A), originated at the contact between doleritic dike and intruded carbonate sediments. This am-phibolite is composed of Brs, Ab, Ep, phengite (Ph) and rutile (Rt). Abbreviations according to Kretz (1983).

Table 1 - Petrographic characterization and geographic location of the meta-mafic rocks from the Sierra de Baza.

Sample	Protolith	Metamorphic assemblage	Metamorphic texture	Metamorphic rock	Longitude	Latitude	Elevation
Cani-5B	Gabbro	Amp Na-Ca, Ab, Ep, Rt, Ttn, Mt	Porphyroblastic	Ab-Ep Amphibolite	520700	4131833	1527
Cani-5C	Gabbro	Amp Na, Ab, Ep, Rt, Ttn, Mt	Porphyroblastic	Ab-Ep Amphibolite	520700	4131833	1527
Cani-22	Dolerite	Brs, Hbl, Czo, Ab, Bt, Rt, Mt, Carb Fe	Porphyro-nematoblastic	Ab-Ep Amphibolite, Amphib. Calcschists	521062	4131764	1519
Cani-23	Dolerite	Brs, Ab, Ep, Mt, Rt, Chl	Grano-porphyroblastic	Ab-Ep Amphibolite	521146	4131765	1504
Cani-31	Basalt (sill)	Brs, Ab, Ep, Chl, Rt	Nematoporphyroblastic	Ab-Ep Amphibolite	518003	4131227	1483
Cani-35A	Dolerite	Amp Ca, Zo-Czo, Ab, Rt	Porphyro-nematoblastic	Ep Amphibolite	520764	4131851	1530
Cani-42	Basalt (sill)	Brs, Zo-Czo, tg, th, Ab, Ep, Chl, Rt	Nematoblastic	Ab-Ep Amphibolite	521276	4131720	1484
Cani-43	Basalt (sill)	Prg, Mg-Ktp, Ab, Czo, Rt, Ed, Carb, Sd	Grano-porphyroblastic	Ab-Ep Amphibolite	521276	4131720	1484
Cani-48	Dolerite	Amp Ca, Ab, Zo-Czo, Alm, Chl, Rt	Porphyroblastic	Garnet-epidote amphibolite	520592	4131594	1532
Cani-83	Px-Ol gabbro	Gln, Ab, Czo, Prg, Alm, Brown amp, Bt, Ilm, Rt, Ttn, Zrn	Granoblastic	Ab-Ep Amphibolite	520831	4133235	1238
Cani-136B	Basalt	Amp Ca, Ab, Ep, Rt, Mt, Qtz	Granonematoblastic	Ab-Ep Amphibolite	505157	4127561	1462
Cani-136C	Basalt	Omp, Alm, Amp Na-Ca, Czo, Ilm, Rt, Ab, Ph	Porphyro-nematoblastic	Eclogite	505157	4127561	1462
Cani-137A	Ferrogabbro-ferrodolerite	Gln, Omp, Rt, Alm, Ab, Ep, Qtz	Porphyroblastic	Garnet-epidote amphibolite	505046	4127410	1471
Cani-137B	Ferrogabbro-ferrodolerite	Gln, Omp, Rt, Alm, Ab, Ep, Qtz	Porphyroblastic	Garnet-epidote amphibolite	505046	4127410	1471
Cani-138	Basalt	Gln, Omp, Rt, Alm, Ttn	Porphyroblastic	Partially amphibolitized eclogite	506648	4127121	1602
Cani-139A	Px gabbro	Omp, Gln, Ab, Alm, Czo, Rt, Ilm, Carb, Colorless Mica	Porphyroblastic, Coronitic	Coronitic eclogite	506648	4127121	1602
Cani-139B	Px gabbro	Omp, Alm, Ab, Zo-Czo, Rt, Ilm	Coronitic	Coronitic eclogite	506648	4127121	1602
Cani-139C	Px gabbro	Omp, Amp Na-Ca, Ab, Alm, Rt, Czo, Bt, Ep	Porphyroblastic	Eclogite	506648	4127121	1602
Cani-250B	Dolerite	Gln, Alm, Rt, Amp Na-Ca, Ep, Colorless Mica	Porphyroblastic	Partially amphibolitized eclogite	508220	4127843	1597
Cani-253	Basalt (Pillow lava)	Amp Ca, Ab, Cpx, Ep, Carb	Porphyroblastic	Ab-Ep Amphibolite	509408	4128745	1662
Cani-281	Basalt	Amp Ca, Ep, Colorless Mica, Rt, Chl., Ttn	Nematoblastic	Epidote amphibolite	521058	4131511	1515
Cani-282	Basalt	Zo-Czo, Ab, Chl, Carb	Nematoblastic	Epidotite	521058	4131511	1515
Cani-285	Basalt	Amp Ca, Ep, Colorless Mica, Chl	Nematoblastic	Epidote amphibolite	513801	4128228	1749
Cani-288A	Dolerite (sill)	Amp Ca, Ep, Ab, Rt, Czo, Chl, Ttn, Zrn	Nematoblastic	Epidote amphibolite	513801	4128228	1749
Cani-298	Px gabbro	Omp, Alm, Amp Na-Ca, Czo, Llm, Rt, Ep	Porphyroblastic	Eclogite	508064	4127586	1557
Cani-300	Ferrodolerite	Gln, Brs, Ktp, Ab, Rt, Ep, Chl, Ilm, Qtz	Porphyroblastic	Ab-Ep Amphibolite	507928	4127809	1519
Cani-303	Basalt (sill)	Ep, Ab, Brs, Amp Na-Ca, Alm, Chl, Rt, Ilm, Bt, Qtz	Porphyro-nematoblastic	Epidote amphibolite	505109	4127255	1462
CH-10A	Gabbro	Omp, Amp Na, Rt, Ep, Ab	Porphyroblastic	Amphibolitized eclogite	506648	4127131	1598
CH-12	Px basalt	Gln, Alm, Rt, Ky, Gln, Ab, Ep	Porphyroblastic	Partially amphibolitized eclogite	506648	4127131	1598
CH-12B	Px basalt	Gln, Czo, Brown amp, Rt, Ab, Chl	Porphyroblastic	Ab-Ep Amphibolite	506648	4127131	1598
CH-21	Dolerite	Amp, Ab, Ep, Rt, Mt, Chl, Ap	Nematoblastic	Ab-Ep Amphibolite	513783	4128225	1741
CH-30	Basalt	Omp, Alm, Czo, Trm, Ab, Pg, Rt, Ilm	Porphyroblastic	Eclogite	507498	4126095	1462
CH-40	Basalt	Alm, Omp, Prg, Ktp, Trm, Ab, Zo-Czo, Rt, Brs, Ky, Act, Pg, Ph	Porphyroblastic	Ab-Ep Amphibolite	507498	4126095	1462
CH-43	Ol gabbro	Omp, Brs, Trm, Alm, Ilm, Ab, Czo, Rt	Coronitic	Partially amphibolitized coronitic eclogite	507638	4126457	1482
CH-44	Ol-Px gabbro	Amp Na-Ca, Alm, Czo, Ab, Ilm, Rt, Colorless Mica	Coronitic	Partially amphibolitized coronitic eclogite	507638	4126457	1482
CH-58	Dolerite	Omp, Alm, Amp Na-Ca, Czo, Ilm, Rt, Ep	Coronitic	Coronitic eclogite	507690	4126511	1462
CH-62	Px dolerite	Gln, Alm, Omp, Ab, Czo, Brown amp, Ilm, Rt	Coronitic	Coronitic eclogite	507761	4126185	1429
RA-33A	Basalt (Pillow lava)	Amp Na, Alm, Omp, Rt, Ilm, Czo, Ab	Porphyroblastic	Eclogite	507724	4126356	1452
RA-33B	Basalt (Pillow lava)		Porphidoblastic	Eclogite	507724	4126356	1452

Mineral Abbreviations according to Kretz (1983). Ab- albite; Act- actinolite; Alm- almandine; Amp- amphibole; Brs- barroisite; Bt- biotite; Carb- carbonate; Chl- chlorite; Cpx- clinopyroxene; Czo- clinozoisite; Ed- edenite; Ep- epidote; Gln- glaucophane; Hbl- hornblende; Ilm- ilmenite; Ktp- katophorite; Ky- dysthene; Mic- colorless mica; Mt- Magnetite; Omp- omphacite; Ph- phengite; Pg- paragonite; Prg- pargasite; Qtz- quartz; Rt- rutile.; Sd- siderite; Trm- tremolite; Ttn- titanite; Zo- zoisite; Zrn- zircon.

Table 2 - Petrographic characterization and location of the meta-ultramafic rocks from Sierra de Baza.

Sample	Protolith	Metamorphic assemblage	Metamorphic texture	Metamorphic rock	Longitude	Latitude	Elevation
Cani-4A	lherzolite	Atg, Tr, Chr Mt, Chl, Carb	Porphyroblastic, veined	Serpentinite	521407	4131896	1520
Cani-4C	harzburgite	Atg, Chr, Mt, Tr	Porphyroblastic, veined	Serpentinite	521407	4131896	1520
Cani-4D	harzburgite	Atg, Tlc, Chr Mt, Tr	Porphyroblastic	Serpentinite	521407	4131896	1520
Cani-4E	harzburgite	Atg, Chr Mt, Tur, Pist, Di, Rt, Chl Mg	Granoblastic	Serpentinite, chlorite schist	521407	4131896	1520
Cani-52	harzburgite	Atg, Mt	Porphyroblastic	Serpentinite	519771	4131410	1615
Cani-53	harzburgite	Atg, Tlc, Mt, Chl	Porphyroblastic, veined	Serpentinite	519898	4131438	1589
Cani-119	lherzolite	Atg, Di, Mt,, Tr	Porphyroblastic	Serpentinite	514465	4128214	1754
Cani-277	harzburgite	Atg, Chr, Mt, Tlc, Pen, Clc, Ilm, En	Porphyroblastic, veined	Serpentinite	521261	4131697	1526
Cani-284	lherzolite	Atg, Chr, Mt, Ilm, Ti-Chu, Pen, Di, Aug, Ol	Porphyroblastic	Serpentinite	513801	4128228	1749
Cani-295	harzburgite	Atg, Chr, Mt, Tlc, Ilm, Tr	Porphyroblastic	Serpentinite	508223	4127622	1582
Cani-305	harzburgite	Atg, Chr, Mt, Chl, Tlc, Ilm	Porphyroblastic	Serpentinite	505139	4127188	1476
CH-25	harzburgite	Atg, Ilm, Tr, Rt	Porphyroblastic	Serpentinite	513801	4128228	1749
CH-27	lherzolite	Atg, Chr, Mt, Tur, Tlc, Chl	Porphyroblastic, veined	Serpentinite	513801	4128228	1749
CH-80	harzburgite	Atg, Mt, Tr, Tlc, Chl, Act	Porphyroblastic, veined	Serpentinite	503737	4127681	1424
CH-84	lherzolite	Atg, Chr, Mt, Di, Rt, Chl	Porphyroblastic, veined	Serpentinite	511850	4127175	1678
CH-84B	lherzolite	Atg, Tr, Ilm	Porphyroblastic	Serpentinite	511850	4127175	1678

Mineral Abbreviations according to Kretz (1983): Act- actinolite; Atg- antigorite; Aug- augite; Carb- carbonate; Chl- chlorite; Chr Mt- chromium magnetite; Clc- clinochlore; Di- diopside; En- enstatite; Ol- olivine; Pen- penninite; Pist- pistacite; Rt- rutile; Tcl- talc; Trm- tremolite; Tur- tourmaline.
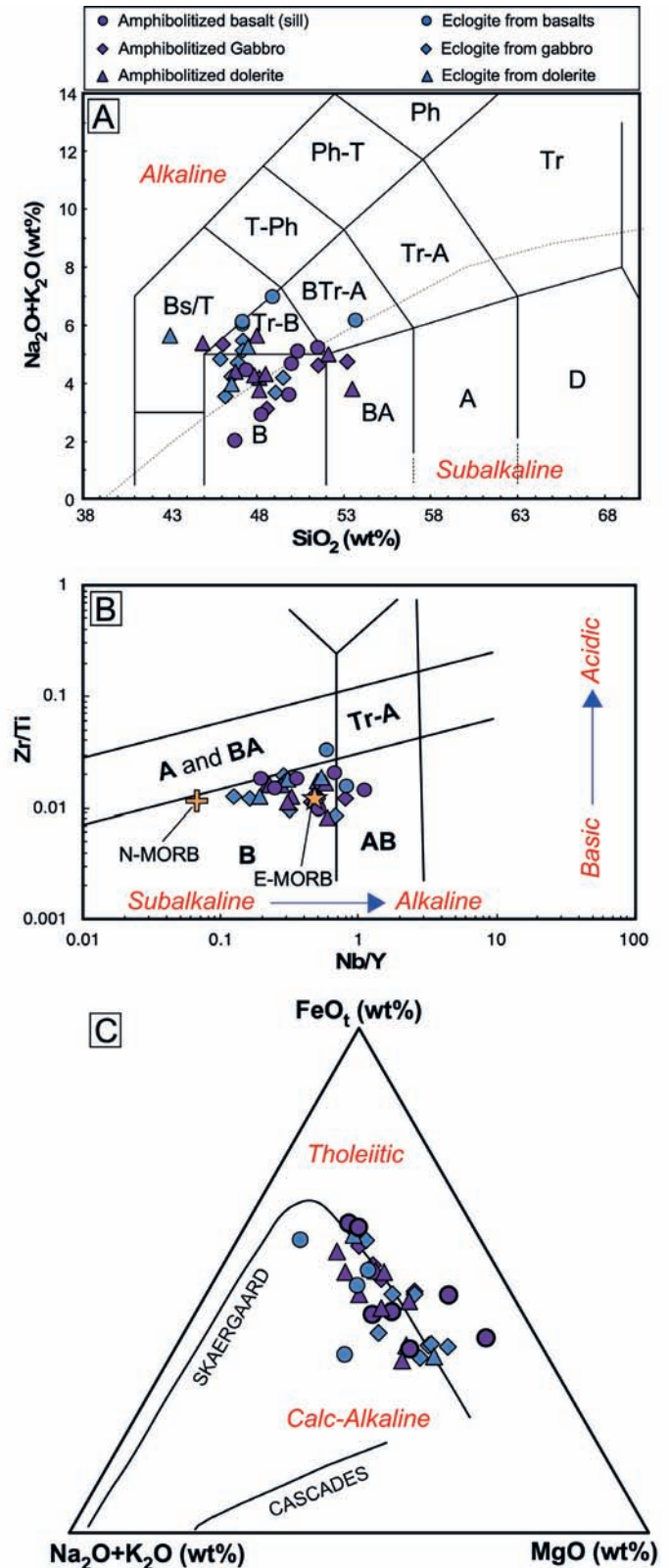
Fig. 3 - Geochemical affinity of the Sierra de Baza meta-mafic rocks, based on: A) Total Alkali-Silica (TAS) binary diagram (Le Bas and Streckeisen, 1991), B) Nb/Y *vs* Zr/Ti binary diagram (Pearce, 1996, modified from Floyd and Winchester, 1975) and C) FeOt-(NaO+K$_2$O)-MgO ternary diagram (Irvine and Baragar, 1971). B- basalt; BA- basaltic andesite; A- andesite; D- dacite; Tr-B- trachybasalt; BTr-A- basaltic trachyandesite; Tr-A- trachyandesite; Tr- trachyte; Bs/T- basanite/tephrite; T-Ph- tephritic phonolite; Ph-T- phonolitic tephrite; Ph- phonolite; AB- alkaline basalt.

Table 3 - Major and trace element composition of the Sierra de Baza meta-gabbros and meta-ferrogabbros.

Metamorphic Rock	Meta-gabbros										Meta-ferrogabbros	
Protolith	Ab+Ep amphibolite Gabbro	Ab+Ep amphibolite Gabbro	Ab+Ep amphibolite Px-Ol gabbro	Eclogite Px gabbro	Cor. Eclogite Px gabbro	Eclogite Px gabbro	Amph. Eclogite Gabbro	Cor. Eclogite Gabbro	Cor. Eclogite Px-Ol gabbro	Eclogite Px gabbro	Amphibolite Ferrogabbro	Cor. Eclogite Ferrogabbro
#	18	19	20	21	22	23	24	25	26	27	28	29
Sample	Cani-5B	Cani-5C	Cani-83	Cani-139A	Cani-139B	Cani-139C	CH-10A	CH-43	CH-44	Cani-298	Cani-137A	Cani-137B
SiO_2 (wt%)	53.33	49.90	47.49	45.93	45.78	46.67	48.92	46.20	48.65	44.84	45.56	46.78
TiO_2	1.85	2.08	1.33	1.11	0.93	1.69	1.46	1.59	1.41	0.83	3.91	3.90
Al_2O_3	13.65	13.90	16.37	16.82	18.16	17.31	16.75	16.59	15.66	19.40	12.66	11.46
$Fe_2O_{3(tot)}$	12.63	13.20	9.93	11.63	8.82	8.95	8.71	9.29	11.53	8.19	14.77	16.49
MnO	0.06	0.07	0.10	0.21	0.14	0.17	0.05	0.16	0.24	0.08	0.15	0.29
MgO	6.54	4.53	6.68	7.17	10.14	6.84	9.19	9.75	7.90	9.24	6.49	5.69
CaO	7.08	8.32	12.53	10.25	11.28	11.24	9.25	10.94	9.90	10.22	9.55	8.57
Na_2O	4.09	4.11	2.88	4.28	3.17	4.18	3.71	3.68	3.29	4.41	4.95	4.88
K_2O	0.63	0.35	0.16	0.29	0.31	1.22	0.39	0.50	0.34	0.30	0.31	0.18
P_2O_5	0.14	0.21	0.16	0.14	0.26	0.49	0.16	0.35	0.10	0.08	0.45	0.77
LOI	0.00	3.32	2.23	1.42	0.41	0.82	1.41	0.38	0.97	1.97	0.83	0.65
Sum	100.00	99.99	99.86	99.25	99.40	99.57	100.00	99.43	99.99	99.55	99.63	99.63
Rb (ppm)	4.42	1.71	0.82	2.98	1.39	15.5	2.16	3.16	4.06	4.12	2.05	1.51
Sr	217	217	781	58.1	345	bdl	180	151	135	214	bdl	74.0
Ba	158	89.9	58.1	1691	62.5	bdl	44.5	22.4	205	9.52	bdl	135
Sc	47.8	51.7	33.0	28.6	18.9	bdl	26.3	32.4	34.1	20.9	bdl	62.7
V	263	307	187	177	132	228	168	187	201	116	870	815
Cr	289	337	377	397	631	317	300	461	294	387	150	150
Co	51.1	71.6	45.4	33.9	34.5	bdl	60.6	76.5	123	52	bdl	61.2
Ni	34.1	22.3	83.2	111	238	115	138	226	114	282	87.0	33.0
Cu	11.6	17.1	8.70	7.20	32.1	bdl	3.60	6.54	5.10	7.18	0.00	6.00
Zn	10.8	20.7	1.50	36.0	53.6	bdl	13.7	45.5	16.2	27.6	102	100
Y	12.6	35.0	17.4	20.2	13.7	18.0	13.9	22.2	18.6	15.7	33.5	57.0
Nb	10.0	17.0	8.00	3.24	3.88	bdl	9.40	6.50	5.80	1.94	bdl	28.9
Ta	0.38	0.99	0.25	0.28	0.36	0.43	0.26	0.65	0.30	0.22	0.49	0.54
Zr	131	162	89	79	106	153	72	165	79	62	206	282
U	0.22	0.44	0.21	0.10	0.06	0.44	0.23	0.13	0.21	0.22	0.37	0.41
Th	2.24	2.05	0.27	0.27	0.22	0.91	0.35	0.35	0.27	0.13	0.89	1.31
Pb	4.00	4.70	4.70	0.58	0.98	bdl	0.80	0.38	1.00	1.08	bdl	1.80
La	2.76	10.29	5.43	1.79	4.46	15.3	5.16	7.72	4.18	3.11	11.4	14.6
Ce	6.55	22.6	13.3	4.30	11.0	27.4	11.4	19.3	10.3	8.33	28.3	35.4
Pr	0.93	2.97	1.88	0.63	1.53	4.07	1.57	2.70	1.55	1.29	4.16	5.11
Nd	4.53	13.52	9.26	3.18	7.02	15.71	7.63	12.4	8.06	6.50	21.3	25.8
Sm	1.34	3.62	2.63	1.16	1.82	4.55	2.16	3.29	2.69	1.98	6.30	7.37
Eu	0.45	1.13	1.06	0.27	0.77	1.44	0.90	1.35	1.18	0.86	1.95	2.16
Gd	1.54	4.24	2.93	1.84	2.03	4.28	2.35	3.60	3.21	2.32	6.66	8.00
Tb	0.33	0.92	0.59	0.38	0.34	0.77	0.46	0.58	0.65	0.40	1.25	1.63
Dy	1.99	5.57	3.21	3.09	2.07	3.88	2.46	3.67	3.50	2.70	6.39	9.14
Ho	0.46	1.28	0.67	0.72	0.47	0.77	0.52	0.78	0.72	0.58	1.32	2.00
Er	1.41	3.72	1.80	1.90	1.26	1.97	1.37	2.11	1.93	1.56	3.50	5.57
Tm	0.25	0.63	0.28	0.30	0.21	0.31	0.21	0.33	0.30	0.23	0.56	0.91
Yb	1.54	3.73	1.60	1.80	1.21	1.77	1.15	1.94	1.80	1.37	3.20	5.42
Lu	0.21	0.51	0.22	0.26	0.17	0.24	0.16	0.29	0.25	0.20	0.47	0.80

Table 4 - Major, trace element composition of the Sierra de Baza meta-dolerites and meta-ferrodolerites.

Metamorphic Rock	Meta-dolerites											Meta-ferrodolerites
Protolith	Ab+Ep amphibolite Dolerite	Ab+Ep amphibolite Dolerite	Ab+Ep amphibolite Dolerite	Ab+Ep amphibolite Dolerite	Ep amphibolite Dolerite	Amph. Eclogite Dolerite	Ep amphibolite Dolerite	Ep amphibolite Dolerite	Ab+Ep amphibolite Dolerite	Eclogite Dolerite	Eclogite Dolerite	Ab+Ep amphibolite Ferrodolerite
#	30	31	32	34	35	36	37	38	39	40	31	42
Sample	Cani-22	Cani-23	Cani-35A	Cani-48	Cani-95	Cani-250B	Cani-285	Cani-288A	CH-21	CH-58	CH-62	Cani-300
SiO_2 (wt%)	44.90	47.00	52.27	47.25	46.67	42.65	46.10	47.67	50.87	46.67	45.81	44.28
TiO_2	1.68	1.29	1.16	2.01	0.99	1.33	1.88	2.30	2.18	1.51	1.33	3.24
Al_2O_3	19.69	19.75	12.08	15.99	19.89	15.68	17.91	16.81	16.79	15.83	18.23	13.93
$Fe_2O_{3(tot)}$	9.99	8.45	10.01	11.14	6.17	17.26	11.42	10.12	10.58	9.13	7.79	15.32
MnO	0.21	0.08	0.18	0.17	0.10	0.40	0.11	0.16	0.14	0.20	0.12	0.10
MgO	2.99	5.38	4.43	5.60	6.61	5.19	7.97	4.76	4.05	8.81	9.10	7.67
CaO	11.92	11.34	13.61	10.25	12.66	9.30	5.13	12.99	7.74	10.54	11.67	8.37
Na_2O	3.08	2.92	3.67	5.30	4.09	5.15	3.55	3.53	4.70	4.13	3.54	4.87
K_2O	1.11	1.14	0.04	0.24	0.05	0.44	0.55	0.17	0.16	1.03	0.38	0.41
P_2O_5	0.36	0.17	0.02	0.35	0.16	1.58	0.30	0.38	0.26	0.31	0.32	0.32
LOI	3.77	2.48	2.54	1.39	2.39	0.77	5.07	0.89	2.54	1.19	0.98	0.69
Sum	99.69	100.00	100.01	99.70	99.77	99.73	99.99	99.78	100.01	99.34	99.25	99.20
Rb (ppm)	20.7	19.7	0.24	2.38	0.45	2.43	5.17	1.54	3.66	9.42	1.47	3.55
Sr	573	934	312	185	412	60.2	209	393	282	176	468	132
Ba	201	125	35.5	15.1	10.8	bdl	89.5	10.3	123	97.2	132	54.6
Sc	31.9	21.0	32.9	39.2	18.8	bdl	29.4	35.1	36.4	28.4	24.2	50.0
V	206	165	186	265	129	174	255	242	316	174	149	378
Cr	253	238	324	297	446	331	230	183	94.7	499	293	26.7
Co	58.9	48.9	86.2	44.1	50.9	bdl	54.2	55.0	53.6	86.7	85.7	79.5
Ni	90.1	76.4	138	129	172	0.00	311	117	184	195	207	233
Cu	162	3.60	5.10	8.53	43.9	0.00	66.0	29.5	114	6.71	26.4	28.0
Zn	51.7	24.6	113	68.6	43.7	0.0	94.3	102	171	47.8	56.4	81.5
Y	24.3	24.6	16.3	39.5	16.2	116	32.5	35.2	35.7	23.7	19.0	28.6
Nb	12.1	8.00	9.60	8.80	3.63	22.1	16.2	9.87	20.5	12.9	5.84	8.81
Ta	0.94	0.16	0.36	0.71	0.36	0.33	0.25	0.81	1.04	1.12	0.60	0.62
Zr	124	95	56	200	92	100	194	218	218	170	140	212
U	0.27	0.32	0.29	0.25	0.13	0.04	0.55	0.34	0.54	0.22	0.12	2.06
Th	0.74	0.51	0.84	0.64	0.47	0.05	0.97	0.60	1.13	0.68	0.33	0.46
Pb	3.21	3.30	10.5	2.27	1.63	bdl	3.60	7.96	37.0	0.61	0.99	3.10
La	9.26	8.73	7.62	8.18	4.70	0.32	11.3	9.22	12.7	9.63	6.89	18.7
Ce	20.1	20.4	17.2	21.3	11.9	0.63	27.8	24.1	27.3	21.8	17.4	38.5
Pr	2.67	2.84	2.07	3.18	1.77	0.09	3.89	3.62	4.19	2.85	2.43	4.48
Nd	12.3	13.5	9.45	15.7	8.62	0.46	18.5	17.0	20.2	12.7	11.1	18.5
Sm	3.55	3.47	2.40	4.71	2.43	0.18	4.93	4.89	5.46	3.21	2.91	4.20
Eu	1.52	1.40	0.79	1.66	0.97	0.11	1.62	1.61	1.75	1.20	1.18	1.48
Gd	3.99	3.77	2.58	5.49	2.74	0.81	5.35	5.61	5.81	3.49	3.17	4.37
Tb	0.66	0.73	0.51	0.92	0.44	0.66	1.06	0.92	1.15	0.57	0.52	0.73
Dy	4.10	3.99	2.75	6.26	2.65	10.20	5.79	6.16	6.36	3.76	3.13	4.85
Ho	0.88	0.86	0.59	1.48	0.56	4.05	1.22	1.34	1.36	0.84	0.68	1.08
Er	2.34	2.34	1.60	4.53	1.45	15.1	3.30	3.58	3.79	2.30	1.78	2.90
Tm	0.36	0.36	0.25	0.66	0.24	2.70	0.52	0.54	0.62	0.36	0.29	0.46
Yb	2.17	1.98	1.43	4.59	1.38	16.01	2.94	3.26	3.67	2.12	1.68	2.66
Lu	0.32	0.26	0.20	0.78	0.19	2.27	0.40	0.48	0.51	0.31	0.25	0.38

Table 5 - Major and trace element composition of the Sierra de Baza meta-mafic rocks.

	Meta-basalts								Meta-basalts (sills)				
Metamorphic Rock Protolith	Ab+Ep amphibolite	Amph. Eclogite	Amphibolite	Ep amphibolite	Eclogite	Ep amphibolite	Ab+Ep amphibolite	Eclogite	Eclogite	Eclogite	Eclogite	Ab+Ep amphibolite	Ab+Ep amphibolite
	Basalt	Basalt	Pillow lava	Basalt	Basalt	Basalt	Basalt	Pillow lava	Pillow lava	Basalt	Basalt	Basalt	Basalt
Sample	Cani-136B	Cani-138	Cani-253	Cani-281	CH-12	CH-12B	CH-40	RA-33A	RA-33B	ELUG-28	AUL-15	Cani-42	Cani-43
#	43	44	45	46	47	48	49	50	51	52	53	54	55
SiO_2 (wt%)	49.43	46.70	50.50	46.26	48.38	49.31	49.46			46.10	53.04	47.41	45.26
TiO_2	2.29	2.18	1.13	1.82	2.30	2.30	1.82			2.12	2.15	1.36	2.49
Al_2O_3	15.46	15.09	14.27	12.49	16.50	15.01	14.26			15.90	15.34	13.88	12.71
$Fe_2O_{3(tot)}$	11.49	12.49	9.43	9.79	7.77	10.01	8.81			15.44	12.60	13.43	14.43
MnO	0.18	0.20	0.10	0.18	0.07	0.05	0.05			0.08	0.11	0.13	0.09
MgO	2.99	5.87	5.99	11.94	6.02	6.91	8.88			6.88	2.19	10.76	4.21
CaO	12.85	9.82	11.10	14.09	10.28	9.90	9.28			4.78	6.25	8.07	11.71
Na_2O	3.42	5.17	4.68	1.84	6.58	4.18	4.64			5.51	5.69	2.45	3.98
K_2O	0.14	0.77	0.41	0.15	0.29	0.40	0.35			0.43	0.36	0.38	0.24
P_2O_5	0.64	0.43	0.22	0.14	0.57	0.36	0.42			0.28	0.85	0.16	0.19
LOI	0.87	0.71	1.82	1.04	0.60	1.57	2.04			1.52	1.19	1.98	4.69
Total	99.75	99.42	99.66	99.73	99.35	100.00	100.01			99.04	99.78	100.01	100.00
Rb (ppm)	1.44	0.10	6.69	6.92	1.64	2.92	1.22			3.33	7.68	3.26	1.66
Sr	190	bdl	553	153	61.6	170	255	132	84.2	150	275	177	195
Ba	39.2	15.0	93.0	3.09	15.0	75.9	59.8	443	634	14.0	26.4	55.0	79.2
Sc	36.4	bdl	39.0	33.8	31.7	36.6	32.0	24.3	26.1	36.8	bdl	33.0	62.3
V	313	284	327	203	246	270	290	145	155	281	188	190	440
Cr	153	355	356	407	108	163	661	218	265	224	91.0	527	113
Co	62.1	bdl	31.9	63.1	77.5	54.8	56.2	96.3	125	179	131	66.5	66.0
Ni	49.4	98.0	85.0	128	110	60.4	120	159	127	77.6	27.0	289	42.7
Cu	46.7	38.0	12.0	50.1	8.60	3.30	4.00	8.34	7.99	10.9	63.0	6.60	3.00
Zn	91.3	35.0	8.00	79.8	48.1	12.2	4.40	33.9	37.1	22.3	79.0	112	9.20
Y	48.4	21.6	22.3	26.6	23.8	20.0	35.9	18.3	18.0	25.4	49.0	20.2	21.3
Nb	9.64	bdl	8.10	6.67	20.1	22.5	24.4	3.74	3.96	10.8	28.8	10.3	11.1
Ta	0.86	0.74	0.36	0.57	1.58	0.75	0.62	0.58	0.64	1.18	2.15	0.14	0.24
Zr	249	182	120	157	207	195	222	20	25	24	417	87	141
U	0.29	0.46	0.51	0.45	1.90	0.93	0.82	0.16	0.04	0.61	1.07	0.61	0.19
Th	0.69	0.81	1.94	0.44	3.57	0.86	1.13	0.74	0.29	0.67	2.71	0.90	0.50
Pb	3.13	bdl	3.30	1.03	1.11	4.00	1.00	1.47	1.04	0.67	12.0	3.50	1.10
La	11.3	9.37	12.33	6.01	29.2	13.5	21.1	6.91	3.32	8.20	29.0	7.15	7.87
Ce	28.5	22.7	26.4	16.0	64.3	29.7	47.0	17.2	8.46	14.8	61.1	15.5	19.0
Pr	4.25	3.09	3.38	2.45	8.19	3.92	6.04	2.55	1.26	2.02	7.83	2.05	2.62
Nd	20.7	14.6	15.0	11.9	34.9	18.0	27.0	12.3	5.48	8.71	33.5	9.76	12.6
Sm	6.18	3.82	3.71	3.63	8.33	4.55	6.43	3.83	1.76	2.39	8.41	2.80	3.34
Eu	2.09	1.25	1.18	1.28	2.37	1.49	2.13	1.34	0.63	1.00	2.96	1.11	1.10
Gd	7.20	3.89	3.96	4.22	7.52	4.60	6.56	4.52	2.42	3.01	8.85	3.28	3.59
Tb	1.18	0.76	0.76	0.71	1.06	0.84	1.24	0.77	0.43	0.54	1.46	0.66	0.72
Dy	8.37	4.08	4.17	4.64	5.13	4.07	6.51	3.88	2.83	3.84	9.60	3.62	3.89
Ho	1.86	0.86	0.88	1.01	0.87	0.76	1.34	0.68	0.66	0.95	1.93	0.76	0.82
Er	5.53	2.31	2.40	2.55	2.08	1.83	3.52	1.97	1.90	2.75	4.89	2.07	2.24
Tm	0.75	0.36	0.37	0.40	0.32	0.26	0.52	0.30	0.29	0.43	0.72	0.33	0.36
Yb	5.22	1.99	2.10	2.29	2.01	1.38	2.80	1.76	1.71	2.70	4.18	1.89	2.07
Lu	0.89	0.26	0.27	0.31	0.28	0.17	0.35	0.27	0.25	0.37	0.60	0.27	0.30

and N-MORB-type mantle sources, irrespective to the superimposed type of metamorphism (Fig. 4B). However, some samples (Cani-5B, Cani-5C y CH-12) show a variable Th enrichment and plot above the MORB-OIB array. In our view, these anomalous samples reflect assimilation of sedimentary components similar in composition to the micaschists from the Sierra de Baza sedimentary sequence (Cani-286) and of the average Global Oceanic Subducting Sediments (GLOSS, Plank and Langmuir, 1998). In Fig. 4C, the Sierra the Baza meta-mafic rocks are plotted in the N-MORB normalized La_N/Sm_N vs La_N/Yb_N binary diagram (normalization values from Pearce, 2008). Most of the samples are characterized by a $(La/Sm)_N$ between 1.0 and 1.8, delineating a compositional trend between LREE-depleted compositions typical of ophiolitic basalts of the Alpine-Apennine domain (e.g., Corsica, Calabria and Platta) and the average of enriched mid Atlantic ridge (E-MAR) basalts from the 63°N (Wood et al., 1979). Only a minor sample subset (CH-12, CH-12B and CH-40) shows distinctive LREE enrichment being characterized by a $(La/Sm)_N$ between 1.8 and 2.1 and by $(La/Yb)_N$ over 5, thus plotting outside from the enrichment trend defined by E-MAR 63°-45°N (Wood et al., 1979). This could result either from the assimilation of sedimentary components, as proposed for the Gets ophiolites (Fig. 4C), by source enrichment, or by a comparatively low melting degree (Bill et al., 2000). In Supplementary Fig. 2A, the Sierra de Baza meta-mafic rocks are plotted in the N-MORB normalized Nb_N vs Th_N tectonomagmatic discrimination diagram for ophiolitic basalts

and meta-basalts (Saccani, 2015). In this diagram, the studied rocks mainly plot across the E-MORB field, with few samples displaced toward the field of N- and G-MORB, the latter indicating garnet-bearing mantle source. Coherently, the Sierra de Baza rocks plotted in the chondrite-normalized $(Dy/Yb)_N$ vs $(Ce/Yb)_N$ diagram of Supplementary Fig. 2B (Saccani, 2015) mainly show an enriched E-MORB affinity, with subordinate samples showing N-MORB and G-MORB geochemical features, respectively.

To have a more general view of the whole trace element distribution, the Primitive Mantle (PM)-normalized distribution of incompatible elements of the meta-mafic rocks of Sierra de Baza is displayed in Fig. 5. The eclogitized (Fig. 5A) and amphibolitized (Fig. 5B) rocks generally show comparable element concentrations. However, a more careful view reveal that significant and distinct LILE distributions characterize the two meta-mafic lithotypes, with the eclogitized samples showing spikes in Ba, and to a lesser extent in Th, and the amphibolitized samples particularly enriched in Pb, and to a lesser extent in Sr. This results in a bimodal distribution in the Ba/Th vs Pb/Th diagram (not shown), with eclogitized samples characterized by very high Ba/Th (up to 6,300, median of 127) and low Pb/Th (median of 2), and amphibolitized samples characterized by relatively low Ba/Th (median of 61) and very high Pb/Th (up to 33, median of 4). These differences may be related to the effect of fluid metasomatism derived from the associated sediments during the different P-T-t paths suffered by these rocks (Breeding et al., 2004).
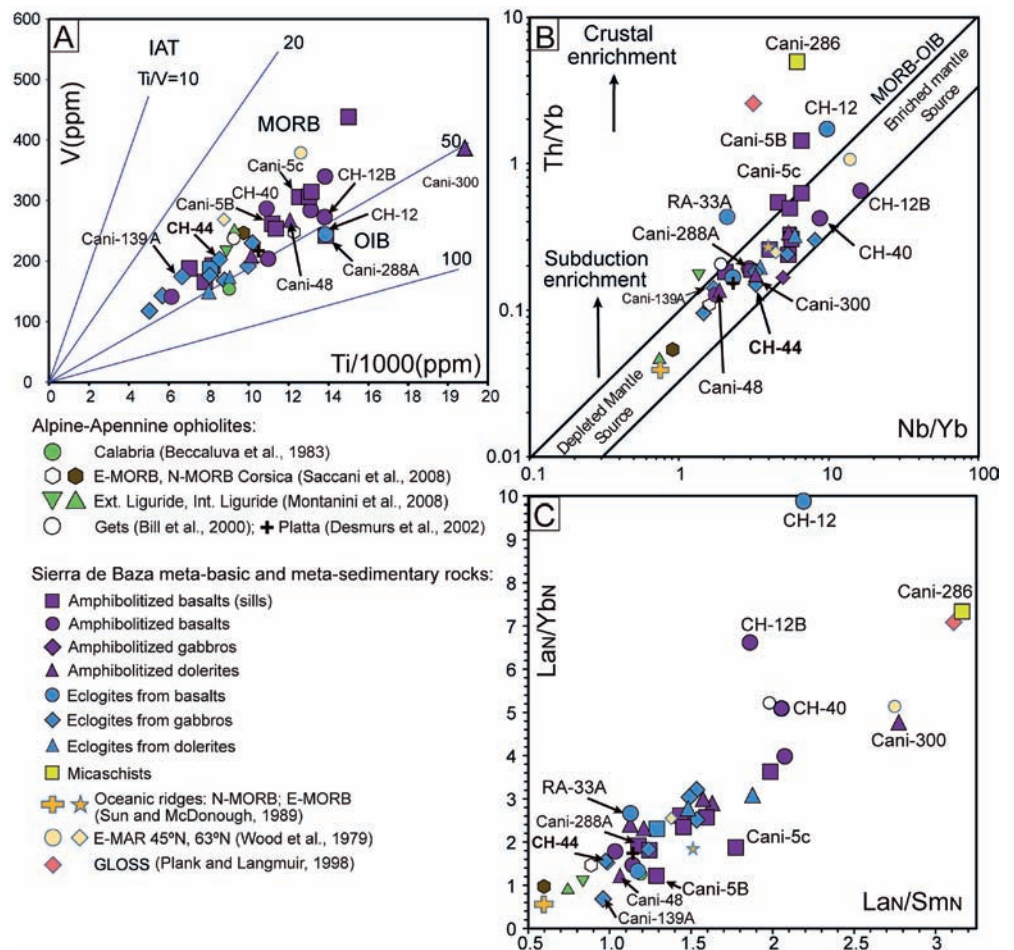

Fig. 4 -Tectonomagmatic discrimination diagrams A) Ti/1000 vs V (Pearce, 2003, modified after Shervais, 1982); B) Nb/Yb vs Th/Yb (Pearce, 1982); C) La_N/Sm_N vs La_N/Yb_N. N-MORB normalizing values are from Sun and McDonough (1989). Larger symbols refer to Sierra de Baza samples.
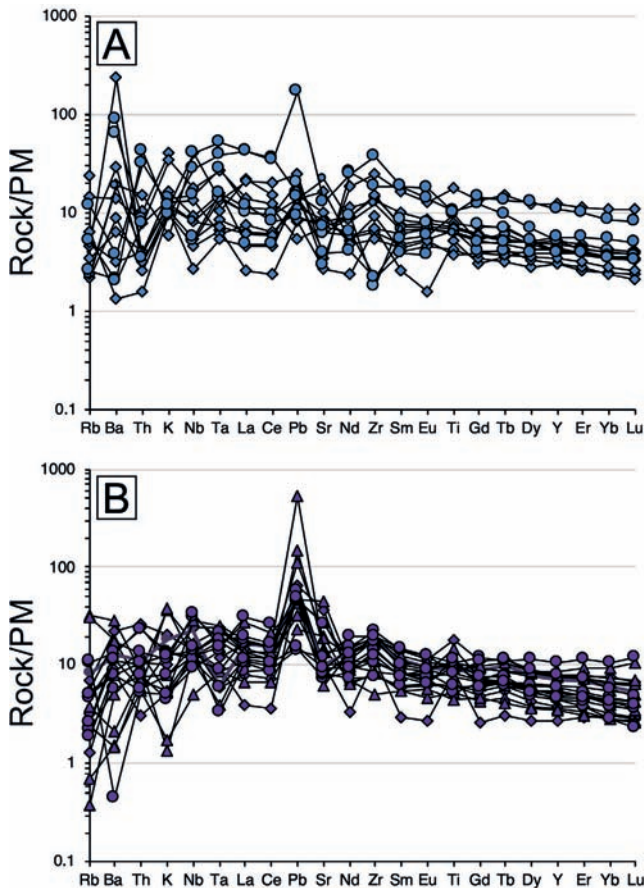
Fig. 5 - PM-normalized incompatible element distribution the of Sierra de Baza meta-mafic a) eclogitized; b) amphibolitized rocks. Normalization values and N-MORB composition are from Sun and McDonough (1989). Symbols as in Fig. 3.

The Sierra de Baza meta-ultramafic rocks

The major and trace elements composition of the meta-ultramafic rocks of the Sierra de Baza is reported in Table 6. CaO vs Al_2O_3 data are compared with other peridotites and serpentinites from the Betic Cordillera and Western Mediterranean ophiolites (Fig. 6). Serpentinized lherzolites are characterized by a limited Al_2O_3 content (3.63-4.31 wt%) coupled with a wider CaO variation (0.80-2.89 wt%), showing a scattered distribution between the trends depicted by Ronda peridotites, the Internal and External Ligurides, clinopyroxene-bearing serpentinites and serpentinized harzburgites from other BOA occurrences (Cerro de Almirez in Sierra Nevada, Puga et al., 1999b). This distribution suggests that cpx-bearing serpentinites derive from lherzolitic lithologies that locally suffered oceanic metasomatism followed by Alpine metamorphism with CaO depletion trending toward the values typical of serpentinized harzburgites. This is supported by the Al_2O_3/TiO_2 ratio (23.4 and 53.3) the average TiO_2 (0.13 wt%) and Cr (2650 ppm) contents (Table 6, see also Beccaluva et al., 1983; Pearce et al., 1984; Puga et al., 1999b; Puga, 2005). Serpentinized harzburgites from Sierra de Baza show an inverse distribution being characterized by very low CaO content (0.02-0.70 wt%) coupled with a wider Al_2O_3 variation (2.31-4.82 wt%) partially overlapping the compositional field of serpentinized harzburgites from Cerro de Almirez (Fig. 6). Noteworthy, serpentinites derive from mantle peridotite rocks that experienced variable fluid/rock interactions, which usually affect FeO and MgO contents (Deschamps et al., 2013). The composition of the Sierra de Baza serpentinites varies between 6.5 and 9.0 wt% and between 35 and 42 wt% for FeO (wt%) and MgO (wt%), respectively (Table 6), overlapping the compositional field of the abyssal peridotites of Niu (2004; Fig. 7A). In particular, the serpentinized harzburgites show a notable dispersion in
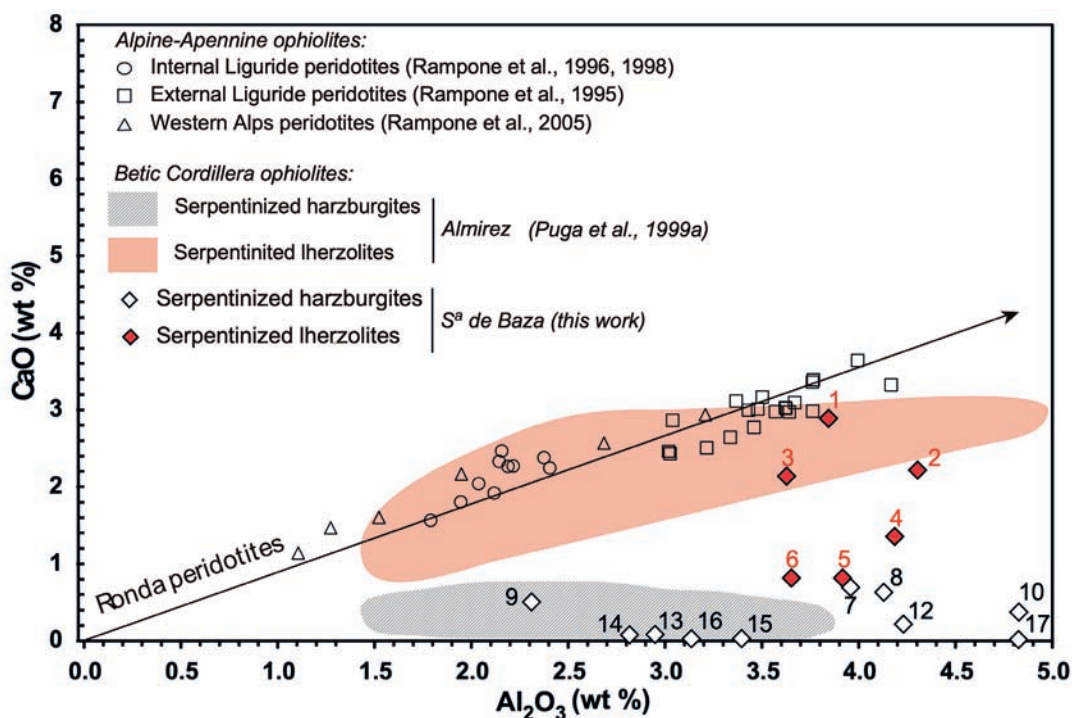

Fig. 6 - CaO vs Al_2O_3 (wt%) binary diagram reporting the compositional variation of Sierra de Baza meta-ultramafic rocks, in comparison with others from BOA (Cerro del Almirez), from Western Mediterranean ophiolitic occurrences (External and Internal Ligúrides, Western Alps), as well as from Ronda peridotite (modified from Puga et al., 1999b).

Table 6 - Major and trace element composition of the Sierra de Baza meta-ultramafic rocks.

	Lherzolite						Meta-ultramafic				Harzburgite					
Protolith #	1	2	3	4	5	6	7	8	9	10	12	13	14	15	16	17
Sample	CH-84B	Cani-04A	Cani-284	CH-27	Cani-119	CH-84	CH-25	Cani-04C	CH-80	Cani-04E	Cani-295	Cani-305	Cani-52	Cani-4D	Cani-53	Cani-277
SiO_2 (wt%)	39.79	42.36	41.23	40.17	41.39	41.20	41.94	41.89	41.16	41.36	41.62	41.19	41.08	46.20	42.23	44.71
TiO_2	0.15	0.13	0.11	0.12	0.07	0.08	0.06	0.09	0.04	0.10	0.08	0.09	0.039	0.15	0.03	0.12
Al_2O_3	3.49	3.88	3.23	3.68	3.47	3.23	3.48	3.65	2.03	4.23	3.75	2.60	2.48	3.04	2.75	4.39
$Fe_2O_{3(tot)}$	12.58	7.37	7.43	8.03	7.19	8.08	6.92	7.15	7.66	7.28	9.03	6.64	7.79	7.74	7.14	8.90
MnO	0.13	0.09	0.11	0.11	0.12	0.18	0.10	0.08	0.05	0.10	0.05	0.12	0.09	0.09	0.05	0.08
MgO	32.16	34.21	35.08	34.61	35.34	35.00	34.84	34.96	36.36	34.44	34.59	37.43	36.56	32.54	35.62	32.78
CaO	2.63	2.00	1.91	1.20	0.71	0.73	0.62	0.62	0.44	0.41	0.19	0.07	0.06	0.03	0.03	0.02
Na_2O	0.02	0.00	0.00	0.00	0.01	0.01	0.00	0.00	0.02	0.00	0.00	0.00	0.00	0.03	0.02	0.01
K_2O	0.01	0.00	0.01	0.00	0.02	0.01	0.00	0.01	0.00	0.03	0.00	0.00	0.00	0.01	0.00	0.00
P_2O_5	0.01	0.00	0.01	0.01	0.02	0.01	0.00	0.01	0.01	0.01	0.01	0.02	0.01	0.01	0.00	0.01
LOI	8.28	10.04	10.20	11.10	11.20	10.80	11.40	10.90	11.50	11.40	9.90	11.20	11.00	9.41	11.40	8.21
Total	99.24	100.04	99.32	99.02	100.21	99.34	99.36	99.35	99.27	99.36	99.22	99.34	99.12	99.23	99.25	99.23
Cs (ppm)	0.01	bdl	0.12	0.05	0.02	0.04	0.16	0.04	0.03	0.14	0.11	0.10	0.04	0.04	0.10	0.13
Rb	0.05	0.08	0.34	0.01	0.07	0.17	0.14	0.17	0.01	1.60	0.28	0.10	0.01	0.01	0.08	1.40
Sr	1.95	4.64	2.10	2.26	1.94	0.89	1.91	1.30	4.24	2.27	1.44	1.04	0.86	4.38	0.77	1.36
Ba	2.76	bdl	4.52	35.0	0.00	60.0	39.0	5.43	1.38	6.90	5.57	1.85	1.87	bdl	1.54	0.86
Sc	bdl	22.3	9.06	bdl	0.00	bdl	bdl	11.5	11.4	16.2	12.6	14.4	bdl	bdl	bdl	15.4
V	117	78.9	66.8	74.0	70.0	66.4	59.3	62.4	70.8	65.8	86.4	56.3	73.2	72.6	76.1	104
Cr	3233	2841	1874	2732	1675	2753	2007	1732	3402	1748	2833	2139	3216	2647	2664	2666
Co	79.0	100	93.1	174	86.0	bdl	128	69.7	97.0	54.8	110	45.7	81.0	98.0	105	62.7
Ni	1599	2097	1894	4229	1492	2019	2200	2054	2199	1169	1891	1631	2676	2161	2126	1421
Cu	62.0	41.4	27.2	64.0	37.0	54.0	105	23.8	5.03	17.0	3.48	30.1	79.0	84.0	81.0	26.2
Zn	97.0	56.7	36.1	69.0	79.0	70.0	84.0	48.0	69.9	69.2	79.4	99.5	77.0	76.0	70.0	87.1
Y	3.19	2.91	2.45	3.25	2.32	3.73	1.06	1.73	0.82	1.85	0.73	1.13	0.57	1.48	1.14	1.67
Nb	0.19	0.13	0.11	0.18	0.13	0.12	0.08	0.10	0.51	0.45	0.26	0.60	0.52	0.38	0.63	0.63
Ta	0.14	0.13	0.05	0.12	0.12	0.13	0.11	0.07	0.18	0.10	0.07	0.08	0.16	0.12	0.13	0.11
Zr	0.58	4.00	1.06	1.02	0.56	0.75	0.80	0.44	0.04	2.42	3.00	4.00	0.01	0.07	0.20	0.55
Hf	0.01	0.03	bdl	bdl	bdl	0.01	bdl	bdl	0.00	0.11	bdl	bdl	bdl	0.01	bdl	bdl
U	0.23	0.09	0.04	0.33	0.11	0.11	0.24	0.09	0.17	0.11	0.08	0.35	0.20	0.18	0.17	0.17
Th	0.11	0.01	0.02	0.03	0.25	0.09	0.03	0.04	2.71	0.41	0.07	0.12	0.09	0.05	0.09	0.31
Pb	0.34	1.50	0.63	0.56	2.00	0.41	1.47	0.33	0.90	1.93	0.37	12.45	0.42	1.33	0.83	0.66
La	0.49	0.18	0.25	0.21	0.91	0.67	0.41	0.18	0.32	0.89	0.13	0.38	0.33	0.09	0.80	0.55
Ce	0.97	0.19	0.48	0.39	2.10	0.56	0.37	0.16	0.76	1.67	0.26	0.69	0.38	0.25	0.31	0.80
Pr	0.19	0.09	0.08	0.09	0.24	0.17	0.11	0.06	0.09	0.21	0.04	0.09	0.08	0.04	0.25	0.12
Nd	0.92	0.54	0.52	0.58	1.02	0.83	0.47	0.35	0.39	0.83	0.17	0.41	0.35	0.21	0.99	0.49
Sm	0.34	0.25	0.17	0.29	0.31	0.30	0.14	0.13	0.09	0.22	0.05	0.11	0.09	0.11	0.21	0.13
Eu	0.09	0.09	0.07	0.10	0.10	0.09	0.05	0.05	0.02	0.05	0.01	0.03	0.02	0.02	0.05	0.03
Gd	0.43	0.34	0.26	0.43	0.36	0.42	0.17	0.20	0.10	0.25	0.09	0.14	0.09	0.15	0.19	0.16
Tb	0.08	0.08	0.05	0.08	0.06	0.07	0.03	0.04	0.02	0.04	0.02	0.02	0.02	0.03	0.03	0.03
Dy	0.54	0.50	0.35	0.55	0.40	0.52	0.18	0.24	0.11	0.26	0.13	0.18	0.09	0.21	0.19	0.21
Ho	0.12	0.11	0.09	0.13	0.09	0.13	0.04	0.06	0.03	0.06	0.03	0.04	0.02	0.05	0.04	0.05
Er	0.34	0.31	0.26	0.38	0.26	0.34	0.12	0.15	0.09	0.17	0.08	0.14	0.06	0.15	0.11	0.15
Tm	0.06	0.05	0.04	0.06	0.04	0.06	0.02	0.03	0.02	0.03	0.01	0.02	0.01	0.03	0.02	0.03
Yb	0.35	0.28	0.23	0.35	0.26	0.36	0.14	0.17	0.11	0.19	0.07	0.16	0.09	0.19	0.14	0.19
Lu	0.05	0.04	0.04	0.05	0.04	0.05	0.03	0.02	0.02	0.03	0.01	0.03	0.01	0.03	0.03	0.03

MgO vs FeO. The observed TiO_2 variation is in the upper range of the abyssal peridotites (Niu, 2004), and partially overlap the field abyssal serpentinites of Deschamps et al., (2013). Serpentinized lherzolites generally have a higher TiO_2 content than serpentinized harzburgites at comparable MgO (Fig. 7B approaching the value of the DM (Salters and Stracke, 2004). The MgO *vs* CaO variation of the Sierra de Baza serpentinites, reported in Fig. 7C, shows two different trends: a) the serpentinized lherzolites characterized by a decrease of MgO in parallel with an increase of CaO,

plotting in the field of the abyssal peridotites and serpentinites (according to Niu, 2004 and Deschamps et al., 2013, respectively), and b) serpentinized harzburgites showing an opposite trend characterized by a marked decrease in CaO coupled to a slight decrease in MgO, possibly caused by intense ocean floor metasomatism, partially overlapping the field of abyssal peridotites (Niu, 2004). Likewise, serpentinized lherzolites from Sierra de Baza have a distinctly higher CaO (> 0.85 wt%) content, with respect to their harzburgitic counterparts (CaO < 0.85 wt%). These latter
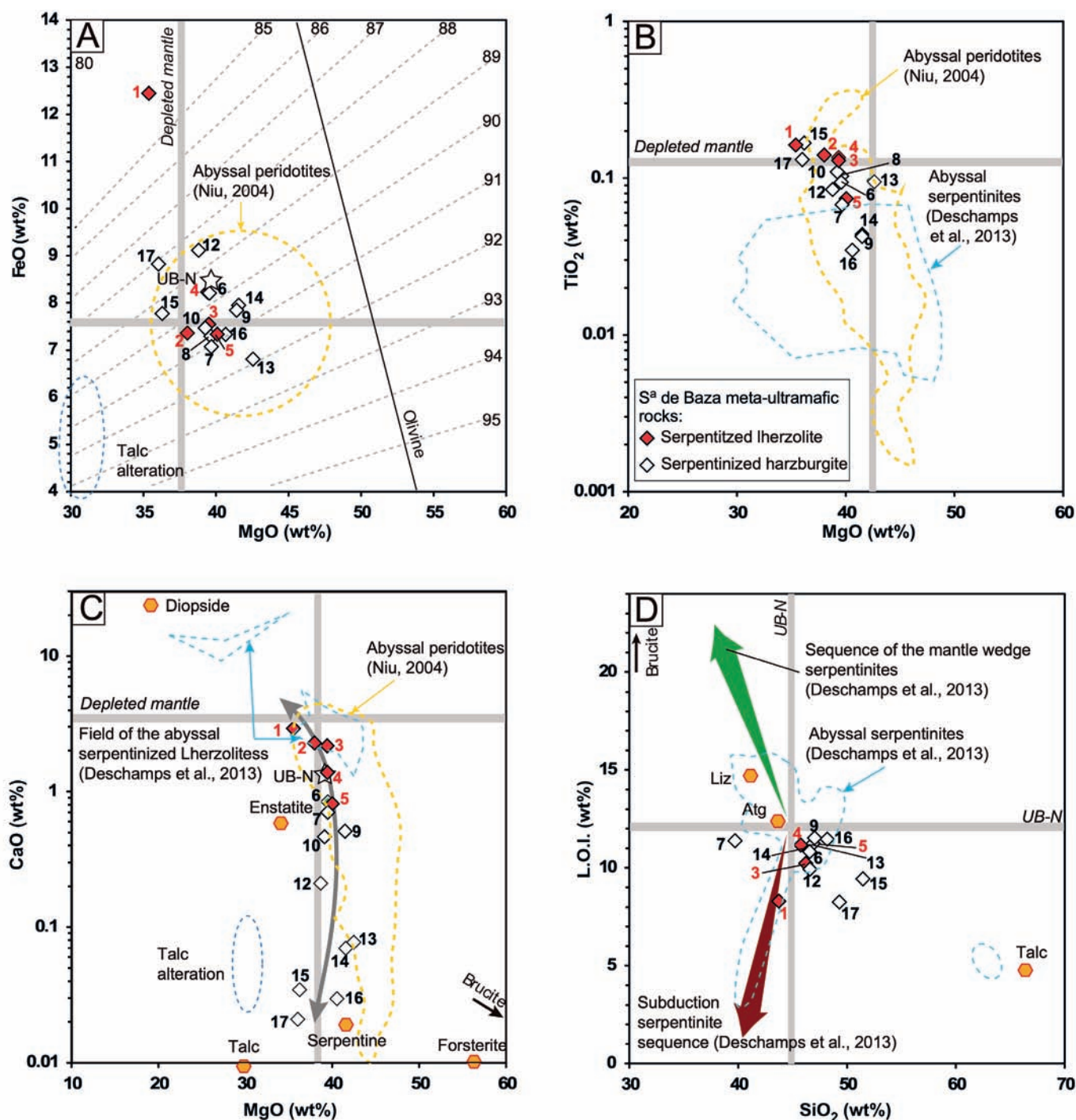

Fig. 7 - Binary diagrams of bulk rock composition (wt%) for Sierra de Baza serpentinites. A: MgO *vs*. FeO; B: MgO *vs*. TiO_2; C: MgO *vs*. CaO; D: SiO_2 against L.O.I. (loss on ignition). Estimated composition of the depleted mantle from Salters and Stracke (2004); compositions of abyssal peridotites from Niu (2004); UB-N international standard composition (star) from Georem (http://georem.mpch-mainz.gwdg.de). Modified from Deschamps et al. (2013).

depict a compositional trend toward low CaO and MgO (wt%) values, compatible with an increasing talc content (sample Cani-4D and Cani-277, Table 6). These features were also observed in the chlorite-bearing serpentinized harzburgites of Cerro del Almirez (Marchesi et al., 2013). The mineralogical variation of the Sierra de Baza serpentinites could be inherited by the pristine composition of the peridotite protoliths (lherzolites and harzburgites) as well as by ocean floor processes leading to tremolite and talc formation, as already observed in the MAR serpentinites (Allen and Seyfried, 2003; Bach et al., 2004; Paulick et al., 2006). The observed CaO depletion is a common feature of serpentinization processes (Coleman, 1977; Janecky and Seyfried, 1986; Miyashiro et al., 1969; Palandri and Reed, 2004), with the exception of local carbonate precipitation, which can increase the CaO content in the rock (e.g., Seifert and Brunotte, 1996). In Fig. 7D the Sierra de Baza samples partially overlap the composition of abyssal serpentinites (Deschamps et al., 2013), showing L.O.I. comparable or lower than the theoretical serpentine minerals (average of 12 ± 3 wt%). The relatively low L.O.I. of the Sierra de Baza samples is incompatible with the presence of secondary brucite (low SiO_2 and very high L.O.I.), a common mineralogical feature of mantle wedge serpentinites (Deschamps et al., 2013). On the other hand, serpentinized harzburgites (in particular samples Cani-4D and Cani-277) show a trend characterized by SiO_2 increase coupled with L.O.I. decrease, typical of talc-bearing abyssal serpentinites. Most of the Sierra de Baza serpentinites are characterized by high bulk rock Al_2O_3/SiO_2 (> 0.05) and low MgO/SiO_2 (< 0.86), similar to the composition of Primitive and Depleted mantle (Supplementary Fig. 3). Serpentinized harzburgites are generally characterized by lower Al_2O_3 contents (samples CH-80, Cani-305, Cani-52, Cani-4D and Cani-53), with respect to serpentinized lherzolites depicting a trend parallel to the oceanic array (Snow and Dick, 1995; Bodinier and Godard, 2003; Niu, 2004). The presence of two samples (Cani-4D and Cani-277) showing comparatively lower MgO/SiO_2 is attributable to their enrichment in talc, a mineral that is commonly produced by the ocean floor metasomatic stage. The serpentinized lherzolites of Sierra de Baza are well clustered in a tight Al_2O_3/SiO_2 range (between 0.078 and 0.09), generally higher than that of serpentinized harzburgites, reflecting their mineralogy that include comparatively higher amounts of chlorite, epidote and the presence in one sample of tourmaline.

The primordial mantle (PM)-normalized incompatible element distribution of the Sierra de Baza serpentinites, shows particular enrichments in Pb and U together with a depletion in HFSE such as Zr and Hf, as well as in Sr (Fig. 8A). Similar elemental enrichments have been observed by other authors in subducted serpentinites (Deschamps et al., 2013). Noteworthy, the serpentinized harzburgites are characterized by lower Sr, Zr and Hf concentrations, and by higher content of U and Pb, with respect to serpentinized lherzolites.

The Chondrite (Ch)-normalized Rare Earth Elements (REE) patterns of the Sierra de Baza serpentinites are showed in Fig. 8B. Both serpentinites derived by lherzolites and from harzburgites show variable negative anomalies in Ce and Eu, the first more pronounced in serpentinized lherzolites and the second in serpentinized harzburgites. In general, the serpentinized lherzolites are richer in HREE with respect to the serpentinized harzburgites, consistent with the different amount of clinopyroxene of the former with respect to the latter.

The serpentinized lherzolites show lower LREE enrichment (La_N/Sm_N = 0.5-1.8) than the serpentinized harzburgites (La_N/Sm_N = 0.5-2.6).

Sr-Nd isotope systematics

The Sr and Nd isotopic composition of the metabasite from Sierra de Baza is reported in Tables 7 and Fig. 9. The $^{87}Sr/^{86}Sr$ varies in the range 0.70384-0.70838, whereas $^{143}Nd/^{144}Nd$ varies between 0.51247 and 0.51306. The meta-mafic rocks are characterized by a significant variation of the Sr (0.70384-0.70600) with respect to Nd (0.51306-0.51278) isotope ratios, whereas the meta-ultramafic sample (Cani-284) show the most radiogenic Sr (0.70838) and the least radiogenic Nd (0.51247) isotope composition. The distribution of Sierra de Baza meta-mafic rocks overlap with the wide range defined by other mafic and ultramafic rocks from alpine ophiolitic occurrences (internal Ligurides: Rampone et al., 1998; Alps: Stille et al., 1989; Platta: Schaltegger et al., 2002), the Mid Atlantic Ridge (Cipriani et al., 2004) and those from other ophiolitic occurrences of the Betic Cordillera (Lugros, Cóbdar, Algarrobo, Cerro del Almirez: Puga et al., 2011; 2017). The Sr isotopic values clearly reflect that the pristine geochemical budget of mantle rocks and mantle derived magmas has been modified, mainly by interaction with sea water during the ocean floor metasomatism, as invariably observed in serpentinites worldwide (Scambelluri et al., 2019).
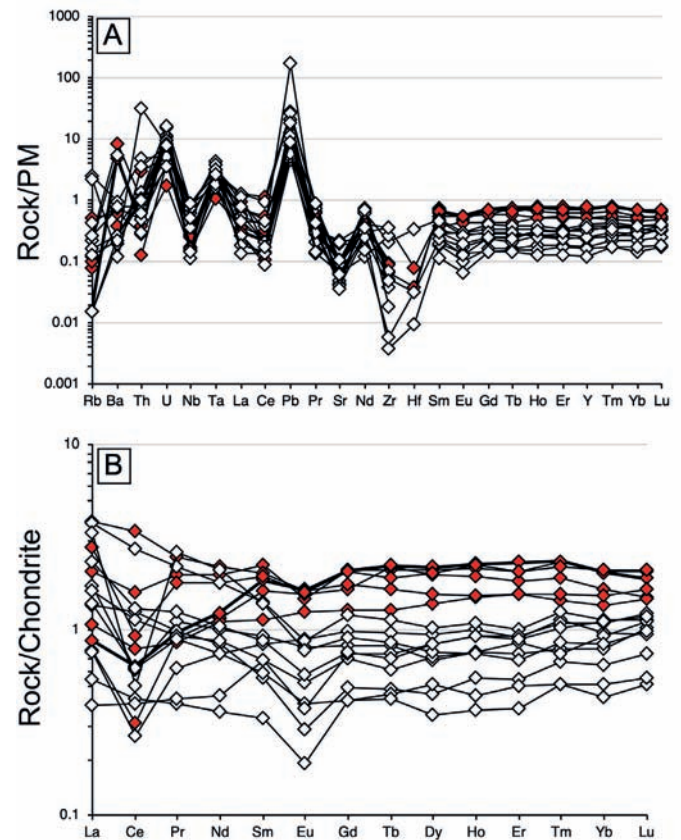

Fig. 8 - (A) Primitive Mantle (PM)-normalized incompatible element and (B) Chondrite (Ch)-normalized REE distribution the of Sierra de Baza serpentinites. Symbols as in Fig. 6. Normalization values are from Sun and McDonough (1989).

Table 7 - Sr-Nd isotope composition of the Sierra de Baza ophiolites.

	Metamorphic Rock	Protolith	#	Sample	$^{87}Sr/^{86}Sr$	$^{143}Nd/^{144}Nd$
Meta-mafic rock						
	Cor. Eclogite	Px-Ol gabbro	26	CH-44	0.70466	0.51305
	Eclogite	Px gabbro	27	Cani-298	0.70542	0.51302
	Ab+Ep amphibolite	Dolerite	32	Cani-35A	0.70627	0.51278
	Ab+Ep amphibolite	Dolerite	39	CH-21	0.70766	0.51298
	Ep amphibolite	Basalt	46	Cani-281	0.70384	0.51306
	Ab+Ep amphibolite	Basalt	49	CH-40	0.70545	0.51301
	Ab+Ep amphibolite	Basalt	54	Cani-42	0.70608	0.51285
Meta-ultramafic rock						
	Serpentinite	Lherzolite	3	Cani-284	0.70838	0.51247

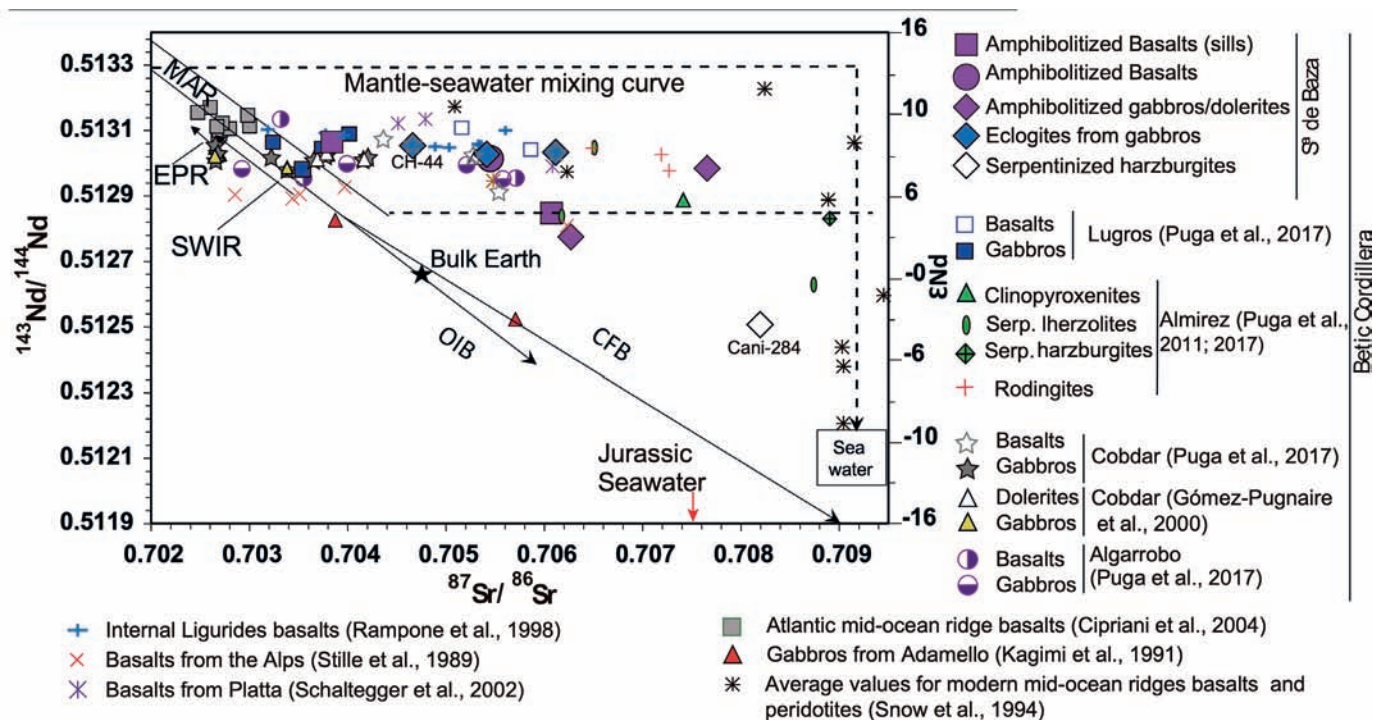Fig. 9 - Present day $^{87}Sr/^{86}Sr$ and $^{143}Nd/^{144}Nd$ isotope composition of metabasite rocks from Sierra de Baza compared with metabasites and meta-ultramafic rocks from other Betic and Alpine ophiolite occurrences and abyssal peridotites (data from Snow et al., 1994). Dotted line represents the mantle-modern seawater mixing curve for abyssal peridotites. Sr-Nd isotopic values of EPR (Eastern Pacific Rise), MAR (Mid-Atlantic Ridge), SWIR (South Western Indian Ridge) and OIB (Oceanic Island basalts) are from Hoffman (1997), whereas CFV (Continental flood basalts) are from Marzoli et al. (1999). Jurassic Seawater composition is from Burke et al. (1992) and Jones et al. (1994), whereas modern seawater is from Snow et al. (1994).

DISCUSSION

Geochemical features of the Sierra de Baza Ophiolites

The meta-ultramafic rocks of Sierra de Baza ophiolitic association show geochemical features typical of seafloor metasomatism, that were mostly preserved during the subsequent metamorphic stages. The variable CaO depletion of serpentinized harzburgites plausibly resulted either by cpx paucity in the pristine peridotite protoliths by high degree partial melting and/or by the breakdown of clinopyroxene during serpentinization in oceanic environment (Bodinier et al., 1993; Puga et al., 1997; 1999b). However, their variable Al_2O_3 content, sometimes higher than that recorded in the associated serpentinized lherzolites, does not support their

genesis by high melting degree of a fertile lherzolite (Fig. 6; Bodinier and Godard, 2003). This is also confirmed by the relatively high Al_2O_3/SiO_2 ratio of the Sierra de Baza serpentinites (Supplementary Fig. 3), which implies their protoliths experienced low partial melting before serpentinization (e.g., Snow and Dick, 1995; Paulick et al., 2006). Similar information derives from the Y vs Ti binary diagram of Pearce and Peate (1995), where Sierra de Baza serpentinites show analogies with peridotites from ridge segments originated by relatively low melting degree (Supplementary Fig. 4). According to Deschamps et al. (2013), in order to highlight the origin and the evolution of the meta-ultramafic rocks from the Sierra de Baza, the ratios of relatively mobile and immobile trace element have been investigated (Fig. 10). The serpentinized

harzburgites invariably show lower values of Yb with respect to serpentinized lherzolites, in agreement with the relative amount of clinopyroxene of the two lithotypes. Their U/Pb distribution is mainly along the magmatic array between the PM and E-MORB mantle domains, well displaced from the field of Tonga forearc harzburgites (Fig. 10A; Deschamps et al., 2013). Among the trace elements, Ti seems to be a useful tracer in the identification of the protolith of the serpentinites, since it is characterized by a limited mobility during serpentinization processes. Mantle wedge peridotite, which experienced extensive partial melting, are characterized by low bulk rock Ti content (Arai and Ishimaru, 2008). Therefore, when plotting the serpentinites on Yb vs Ti diagram, a common positive trend reflects processes of refertilization or depletion by melt extraction, defining distinct fields for the different ultramafic protoliths (Deschamps et al. 2013). In the Ti vs Yb diagram, all the investigated samples plot between the abyssal peridotites, abyssal and subducted serpentinites, showing a decidedly more fertile (or refertilized) composition with respect to mantle wedge serpentinites (Fig. 10B). The Sierra de Baza serpentinites also show lower Sr, Ba, and higher Pb at comparable Yb, concentrations, with respect to mantle wedge serpentinites confirming their geochemical affinity with abyssal peridotites, abyssal and subducted serpentinites (Fig. 10C, D and E). The Pb concentration of the studied serpentinites is always above the PM, in the range of abyssal peridotites and serpentinites, as well as in that of subducted serpentinites (Fig. 10F). Similar information on the origin of the Sierra de Baza serpentinites can be retrieved by the distribution of REE and other incompatible elements. Relevant and discriminant are the normalized ratios between light (L; i.e., La, Ce, Pr, Nd), medium (M; i.e., Sm, Eu, Gd, Tb) and heavy (H; i.e., Tm, Yb, Lu) REE. Serpentinized lherzolite REE patterns do not show peculiar enrichments in LREE (LREE$_N$/HREE$_N$ 0.4-1.9) and nearly flat MREE$_N$/HREE$_N$ (0.9-1.1), whereas serpentinized harzburgites are characterized by a general MREE depletion with respect to LREE and HREE (MREE$_N$/LREE$_N$ 0.4-1.7 and MREE$_N$/HREE$_N$ 0.7-1.1), which has been ascribed to loss of clinopyroxene and plagioclase during pre-orogenic oceanic serpentinization (Puga et al., 1997; 1999b). Noteworthy, the serpentinized lherzolites and harzburgites show REE patterns similar to abyssal and subducted serpentinites, respectively (Fig. 11; Deschamps et al., 2013). In particular, serpentinized harzburgites from Sierra de Baza show LREE enrichment consistent with subducted serpentinized harzburgites (LREE up to ~ 2 Ch). On the other hand, the studied serpentinites differ from mantle wedge serpentinites which show a more depleted composition for both serpentinized lherzolites (LREE up to ~ 1 Ch) and harzburgites (LREE up to ~ 0.2 and HREE up to 0.5 Ch). In other words, Sierra de Baza meta-ultramafic rocks do not share geochemical characteristics with mantle wedge settings, the archetype of which is represented by New Caledonian ophiolites (Secchiari et al., 2016; 2019).

Most of Sierra de Baza serpentinites, show variable Ce and Eu negative anomalies (Fig. 11A, B), that are clearly inherited by seawater (Bau et al., 1995). These geochemical features suggest for a genesis of serpentinites by high seawater/peridotite ratio at relatively low T (< 200°C). On the other hand, the observed REE distribution is inconsistent either with high-T hydrothermalism (Menzies et al., 1993; Allen and Seyfried, 2005) or even with melt-rock interaction (Niu et al., 1997; Rampone et al., 2018) that should produce LREE enrichment coupled with Eu positive anomaly, generally induced by plagioclase crystallization.

The serpentinites of abyssal origin are generated by hydration of the oceanic peridotites by the ocean floor hydrothermal activity, mainly concentrated in the neighboring of the oceanic ridges. After ocean floor metasomatic transformations, some Sierra de Baza serpentinites were affected by metamorphic changes during the subduction process, thus inheriting features typical of "subducted serpentinites" that were recognized in some of the analyzed samples. Subducted serpentinites are formed during convergence as they are associated with other metamorphic rocks of high P-low T (i.e. eclogites) that are also involved in the subduction processes. These genetic hypotheses are corroborated by the distribution of major elements, and of the fluid mobile elements (FME). They are inherited by the composition of the pristine mantle peridotite rocks, by ocean floor metasomatism and also by elemental re-distribution that occur during the complex P-T-t path that interested such rocks during the convergence that preceded the ophiolite obduction. The PM-normalized incompatible element distribution of the Sierra de Baza serpentinites is characterized by enrichments in FME such as Ba, U and Pb and negative anomalies in HFSE (Nb, Zr, Hf) and, to a lesser extent in Sr, which are geochemical features of abyssal and subducted serpentinites (Fig. 11A). On the other hand, mantle wedge serpentinites are characterized by a strong Sr enrichment and LREE depletion, geochemical features not observed in the Sierra de Baza serpentinites.

The enrichment in some FME (e.g., Ba, U, Pb) and depletion in HFSE result from the seawater/rock interactions that take place at mid-ocean ridges, as well as during subduction, by percolation of fluids released from different lithologies of the slab that also include sediments (Deschamps et al., 2013). The subducted serpentinites may be derived either from abyssal or OCT peridotites/serpentinites that, once incorporated into the accretion prism before exhumation, experienced a complex geological history (Deschamps et al., 2011). Chemical interactions occur with various lithologies, in particular with (meta)-sediments, and aqueous fluids, along the entire prograde path. These processes can play an important role in the FME enrichment (Deschamps et al., 2011; Lafay et al., 2013). The interaction of the Sierra de Baza ultramafic rocks with fluids (also containing halogens) is a process also recorded in various serpentinite occurrences world=wide (Bau, 1991; Bau and Dulski, 1995; Haas et al., 1995; Douville et al., 1999; Scambelluri et al., 2004; 2019; John et al., 2011; Kendrick et al., 2011; Marchesi et al., 2013), and is consistent with the presence of F-rich titanium clinohumite in=serpentinized harzburgites from the Cerro del Almirez (López Sánchez-Vizcaíno et al., 2005). The origin of U enrichment (Fig. 10E) observed for subducted serpentinites by Deschamps et al. (2013) can be ascribed to several processes. In the Sierra the Baza case-study, we speculate that U content could be controlled by percolation of fluids derived from sediments that are associated to serpentinites during the formation of orogenic mélanges, as proposed by Cannaò et al. (2015). In other words, part of the serpentinites formed on the ocean floor also suffered further element remobilization and metasomatism, being involved in a complex subduction P-T-t path (Olivier and Boyet, 2006; Deschamps et al., 2010; 2013; Kodolányi et al., 2012).

The meta-mafic rocks of Sierra de Baza ophiolitic association suffered amphibolitization and albitization processes, ultimately leading to Na$_2$O and SiO$_2$ increase with respect to CaO and immobile elements. Therefore, in order
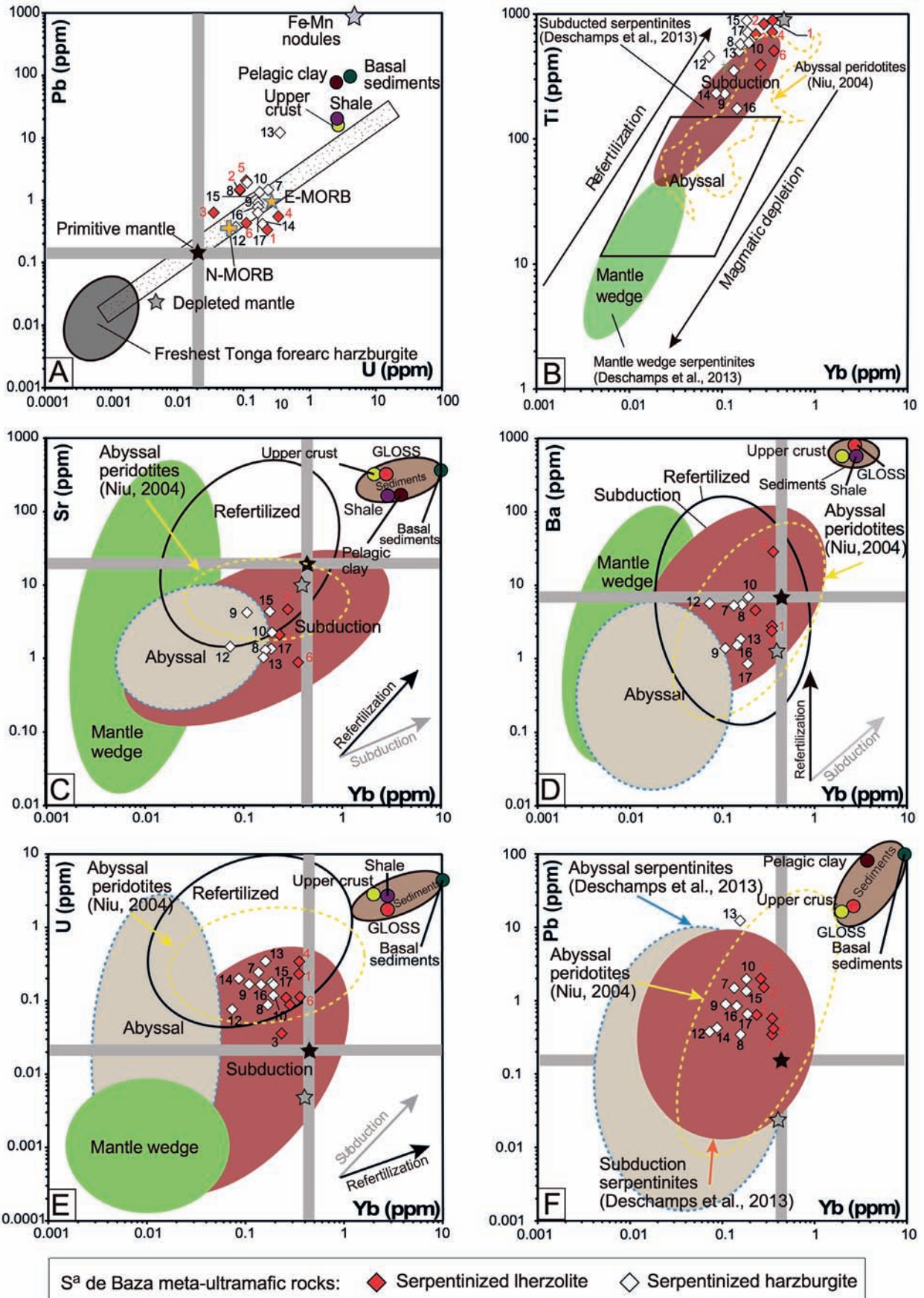
60

Fig. 10 - Whole rock a) U vs Pb, b) Yb vs Ti, c) Yb vs Sr, d) Yb vs Ba, e) Yb vs U, and f) Yb vs Pb variation diagrams reporting the compositional features of serpentinized peridotites of Sierra de Baza. Estimated composition of the depleted mantle from Salters and Stracke (2004); composition of the primitive mantle from McDonough and Sun (1995); compositions of the sedimentary end-members from Li and Schoonmaker (2003); Estimated composition of global subducted sediments (GLOSS) from Plank and Langmuir (1998), modified by Deschamps et al. (2013). Larger symbols refer to Sierra de Baza samples.
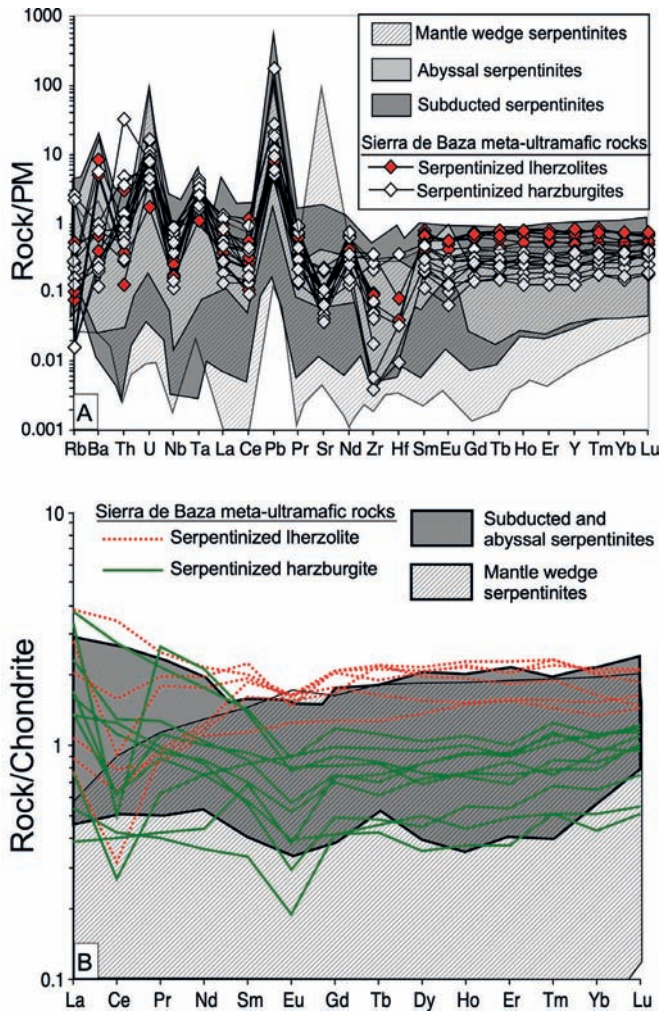
Fig. 11 - (A) PM-normalized incompatible element distribution the of Sierra de Baza meta-ultramafic rocks compared with mantle wedge (Mariana forearc: Parkinson and Pearce, 1998; Kodolányi et al., 2012; Cuba: Marchesi et al., 2006; New Caledonia: Marchesi et al., 2009; Ulrich et al., 2010; South Sandwich arc: Pearce et al., 2000; Savov et al., 2005), abyssal (MAR: Paulick et al., 2006; Jöns et al., 2010; Augustin et al., 2012) and subduction-related (Anatolia: Aldanmaz and Koprubasi, 2006; Betic Cordillera: Garrido et al., 2005; Zagros suture zone: Anselmi et al., 2000; Western Alps: Chalot-Prat et al., 2003; Dominican Republic: Deschamps et al., 2012; Newfoundland: Kodolányi et al., 2012) harzburgitic serpentinites . Normalization values are from Sun and McDonough (1989). (B) Chondrite-normalized REE patterns of meta-ultramafic rocks from Sierra de Baza compared to mantle wedge (Mariana forearc: Parkinson and Pearce, 1998; Kodolányi et al., 2012; Cuba: Marchesi et al., 2006; New Caledonia: Marchesi et al., 2009; Ulrich et l., 2010; South Sandwich arc: Pearce et al., 2000; Savov et al., 2005), abyssal (MAR: Paulick et al., 2006; Jöns et al., 2010; Augustin et al., 2012) and subduction-related (Anatolia: Aldanmaz and Koprubasi, 2006; Betic Cordillera: Garrido et al., 2005) harzburgitic serpentinites. Normalization values are from Sun and McDonough (1989).

to reconstruct their original magmatic affinity, appropriate classification diagrams based on the least mobile elements have been used. On this basis, Sierra de Baza mafic rocks mainly show tholeiitic affinity, with a differentiation trend mainly controlled by olivine/plagioclase fractionation, with a Nb/Y vs Zr/Ti variation mainly between the compositions of N- and E-MORB (Fig. 3B and C). This geochemical affinity is also confirmed by the V vs Ti/1000 diagram

(Fig. 4A), which highlights the presence of a few samples (Cani-300, Cani-288, CH-12) plotting outside the MORB trend. Sample Cani-300 could be interpreted as a more differentiated product along with the tholeiitic trend, which results in the variable enrichment of FeO, TiO_2, Zr, Y and V (Miyashiro, 1975; Beccaluva et al., 1983). This is confirmed by petrographic observation which reports a higher content of rutile aggregates in these rocks, which formed after ilmenite during prograde metamorphism in the eclogite facies, prior to transformation into Ab-Ep amphibolite. Plotted in the Th/Yb vs Nb/Yb (Fig. 4B) and in the $(La/Yb)_N$ vs $(La/Sm)_N$ (Fig. 4C) sample Cani-288 is in the compositional range of N- and E-MORB, likewise most of Sierra de Baza meta-mafic rocks. On the other hand, the Th and La of some samples (including CH-12) highlight a possible contribution of pelitic sediments to a basalt of N-MORB composition (Fig. 4B and C). As proposed above, the Th enrichment, that often occurs together with other lithophile elements, could derive from the assimilation of sedimentary components by MORB-type basaltic magmas during their rise or emplacement in hypabyssal conditions (sills). This is confirmed by the similarity in composition of micaschists from the Sierra de Baza sedimentary sequence (Cani-286) and of the average Global Oceanic Subducting Sediments (GLOSS, Plank and Langmuir, 1998) that can be considered as potential contaminants. The LREE enrichment of a minor sample subset (samples CH-12, CH-12B and CH-40) could result either from the assimilation of pelitic sediment component, as proposed for the Gets ophiolites (Fig. 4C), or also by enrichment, or comparatively low melting degree of the mantle source (Bill et al., 2000). In the N-MORB normalized Nb_N vs Th_N tectonomagmatic discrimination diagram (Supplementary Fig. 2A) proposed by Saccani (2015), most of the Sierra de Baza meta-mafic rocks show E-MORB with minor N- and G-MORB geochemical affinities. This latter sample subset (samples RA-33B, Cani-281, Cani-282, Cani-303, CH-44) display an incompatible element composition similar to N-MORB with TiO_2 (1.08-2.16 wt%), P_2O_5 (0.10-0.22 wt), Zr (76-161 ppm),Y (18.58-48.45 ppm) and by Nb/Y (0.19-0.32) and Ti/V (40.97-53.68) ratios. These rocks have been however interpreted as transitional MORB (T-MORB) due to the comparatively higher Th content and by the LREE/HREE ratio and are plausibly generated by a mantle source slightly enriched during the pristine phases of oceanic opening (e.g., Venturelli et al., 1979). More recently Montanini et al. (2008) and Saccani et al. (2008), observed that similar rocks are also characterized by a comparatively high MREE/HREE ratio ($(Dy/Yb)_N$ from 1.15 to 1.59) with respect to N-MORB ($(Dy/Yb)_N = 1$, Sun and McDonough, 1989), thus ascribing the relative LREE/HREE enrichment mainly to the HREE depletion as a result of the presence of the residual garnet in their mantle sources (Saccani, 2015). In order to better discriminate between normal (N)- and garnet-influenced (G)-MORB source, the Sierra de Baza rocks have been also plotted in the chondrite-normalized $(Dy/Yb)_N$ vs $(Ce/Yb)_N$ classification diagram proposed by Saccani (2015), which confirms that most of the samples have a E-MORB affinity, whereas a sample subset shows garnet-bearing G-MORB geochemical features (Supplementary Fig. 2B).

Chondrite-normalized REE patterns of the Sierra de Baza meta-mafic rocks are shown in Fig. 12, which also reports for comparison the REE distribution of N- and E-MORB (Sun and McDonough, 1989). From this diagram it is evident that the most LREE depleted sample Cani-139A
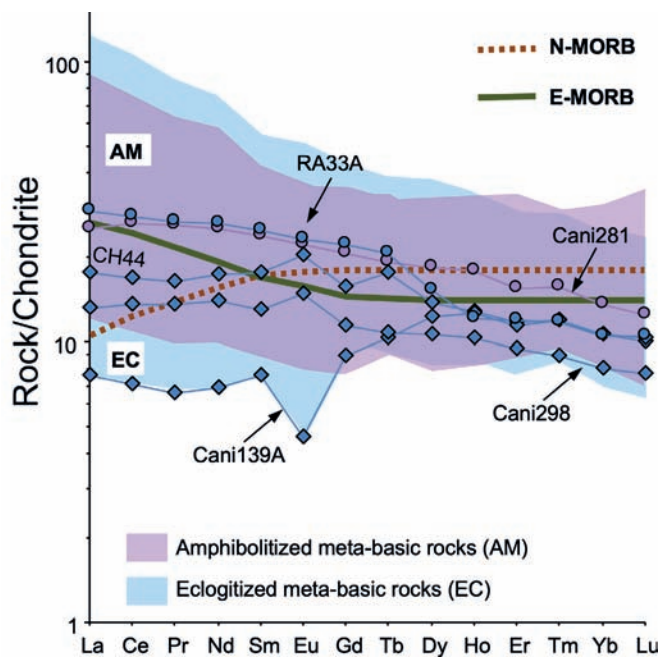
Fig. 12 - Chondrite-normalized REE diagram of the Sierra de Baza metabasites with composition approaching N-MORB and G-MORB fields in Supplementary Fig. 2. Normalization values are from Sun and McDonough (1989).

conforms to the REE distribution of N-MORB, whereas, according to their higher LREE/HREE ratio, samples Cani-281 and RA-33A can be assimilated to that of enriched E-MORB. Samples CH44 and Cani298 show intermediate REE features between E-MORB and N-MORB, plausibly recalling the geochemical features of G-MORB sources, due to their high MREE/HREE which is a feature of residual garnet in the mantle source.

The Sr-Nd isotopic composition of the investigated ophiolite association indicate that meta-mafic and meta-ultramafic rocks variably suffered seawater-rock interaction, with the least altered magmatic rocks showing a MORB-type source and the most altered mantle rocks decidedly trending to the composition of the Tethyan seawater. This trend, which is shared by Alpine ophiolites (Internal Ligurides- Rampone et al., 1998; Alps- Stille et al., 1989; Platta- Schaltegger et al., 2002) and other BOA rocks (Lugros- Puga et al., 2017; Cobdar- Puga et al., 2017 and Gómez-Pugnaire et al., 2000; Algarrobo- Puga et al., 2017; Cerro de Almirez- Puga et al., 2011 and 2017) point to a seawater composition intermediate between the Jurassic (^{87}Sr/^{86}Sr 0.7072-0.7075, Burke et al., 1992, Jones et al., 1994) and modern seawater (^{87}Sr/^{86}Sr 0.7092, Snow et al., 1994). The observed ^{143}Nd/^{144}Nd and ^{87}Sr/^{86}Sr displacement from the MAR array should have been related to the oceanic metasomatism that affected the BOA rocks that was particularly effective on meta-ultramafic rocks and associated rodingite dikes (Puga et al., 2011; 2017).

Age, origin and evolution of the Sierra de Baza ophiolites

The geochemical and isotopic affinity of the different types of mafic rocks of the Sierra de Baza ophiolites, and more in general of the whole BOA mainly correspond to tholeiitic magmatism of T-MORB to E-MORB affinities.

These magma types originated at ocean ridges, such as the Atlantic Ridge, during the incipient oceanization following the continental rifting phase.

In the case of serpentinites generated in abyssal areas, they are generated from oceanic lithospheres associated with slow- (1 to 5 cm / year) to ultra-slow (< 2 cm/year) spreading ridges, which represent approximately one third of the 55,000 km of existing oceanic ridges on a global scale (Dick et al., 2003). These geological settings are characterized by intermittent magmatic and tectonic activity, which cause exposure of the shallow lithospheric mantle during amagmatic periods (Cannat et al., 1995; Karson et al., 2006). The relatively thin oceanic crust (1 to 7 km) and the presence of numerous normal faults on the flanks of the ridge axis promote serpentinization by fluid circulation from the deep oceanic lithosphere (Epp and Suyenaga, 1978; Francis, 1981; Mével, 2003). These abyssal serpentinites represent between 5 and 25% of the Atlantic seafloor (Cannat et al., 1995, Carlson, 2001; Mével, 2003). The exposure of these serpentinites on the ocean seafloor takes place in relation to the following tectonic environments: i) through normal high-angle faults originated from thinning and extension of the oceanic crust along the ridge; ii) in areas of lithospheric denudation due to low-angle faults that expose the lower part of the oceanic lithosphere on the seafloor in the so-called "ocean core complexes" or OCCs (oceanic core complexes: Cannat, 1993; Escartin et al., 2003; Michael et al., 2003; MacLeod et al., 2009); and iii) along large escarpments and transform faults that affect the ridges (Bonatti, 1976; Epp and Suyenaga, 1978; Francis, 1981; Bideau et al., 1991; O'Hanley, 1991; Karson and Lawrence, 1997; Mével, 2003; Morishita et al., 2009; Boschi et al., 2013). In contrast, the fast spreading ridges (> 9 cm / year) have a higher magmatic activity, which results in the formation of a thicker oceanic crust (7-10 km thick). In this framework, the abyssal peridotites would not be exposed on the seafloor (Sinton and Detrick, 1992), thus escaping serpentinization. The serpentinites of Sierra de Baza were subjected to a metasomatic process that transformed lherzolites into serpentinites. These rocks generally still preserved clinopyroxene and other mantle minerals, and include chrysotile or lizardite serpentine, derived by ocean floor metasomatism. Many of them were transformed into secondary harzburgites in a more advanced process of oceanic metasomatism, by destabilization of clinopyroxene and other mantle minerals to cause serpentine, chlorite, talc and iron oxides before undergoing the Alpine subduction process, during which antigorite (high-pressure serpentine polymorph) is formed together with other minerals such as newly formed olivine and enstatite (normally intercropped), in addition to clinohumite, iron oxide and talc.

The rifting process ultimately led to the development of the Tethyan Jurassic ocean basin starting from the Pliensbachian, between 190 and 180 Ma (Puga et al., 2005; 2011 and 2017). Over the last decades, the BOA metamorphic mafic rocks were dated by many (U/Pb, Rb/Sr, K/Ar and Ar/Ar) radiometric methods, which revealed they formed within a wide time span, mainly between the Early and the Late Jurassic (Puga et al., 2017, Table 1). The ocean floor metamorphic stage developed between the Middle and the Late Jurassic (160-150 Ma), close to the end of magmatic phase. The BOA upper age limit (Early Cretaceous) is determined by the extensive development of a sedimentary sequence, superimposed on the igneous materials of the ocean floor, which locally preserves relics of Cretaceous fossils

(Tendero et al., 1993), and is intruded by igneous sills having mineralogical and geochemical composition similar to those of the underlying ophiolitic metabasites (Puga et al., 2011; 2017). These ocean floor sediments mainly represented by siliceous, clayey and carbonated lithologies, which ubiquitously cover both mafic and ultramafic rocks, have been metamorphosed together with the other BOA rocks. Between the Late Cretaceous and the Paleocene (90 to 60 Ma), the approximate limits for the generation of high P (eoalpine) Alpine metamorphism, the igneous lithotypes were transformed into eclogites (Puga et al., 2005; 2011; 2017). However, radiometric datings of the metabasites, demonstrate the existence of at least two more recent stages of retrograde metamorphic recrystallization, 1) a first one of Eocene-Oligocene age (mesoalpine), during which the eclogites are partially transformed into amphibolites and 2) a second one of Middle-Later Miocene age (neoalpine), in the green schist facies (Puga et al., 2017).

Paleogeographic reconstruction of the Betic area

The petrological, geochemical and geochronological similarities between the BOA rocks (including those of Sierra de Baza) and the Alpine-Apennine ophiolites, as well as the paleogeographic reconstructions of the Western Tethys during the Mesozoic, suggest that: a) continental break-up and opening of the Betic Tethys initiated during the Pliensbachien (from 190 Ma), while the Alpine-Apennine Tethys began in the Bathonian (from 170-165 Ma) (Schettino and Turco, 2009, Puga et al., 2011), and b) from the Titonian, the ocean floor generating the Betic and Alpine-Apennine ophiolites formed an oceanic strip, affected by transform faults, that linked the western Tethys and the central Atlantic (Favre and Stampfli, 1992; Guerrera et al., 1993; Schettino and Turco, 2009; Puga et al., 2017). The accretion rate of the ocean floor was around 12 mm/year according to the calculations made by Schettino and Turco (2009; see Puga et al., 2011), typical of ultra-slow spreading ridges, in agreement to the range of radiometric ages of ca. 30 Ma obtained from the beginning to the end of magmatism (Puga et al., 2017). Therefore, the Betic Tethys ocean floor could have reached ca. 200 km of width in the Jurassic, a large part of which would have been subducted during the Cretaceous, without having been exhumed to the surface in the form of eclogites.

Noteworthy, the ultra-slow spreading ridges are characterized by a low melting degree and low volcanic activity (e.g., Basch et al., 2019 and references therein). This generates small and non-continuous volcanic ridges, which are rich in serpentinites, alternated to amagmatic areas along the spreading axis (Michael et al., 2003; Dick et al., 2003). This style of ocean floor propagation is also analogous to processes in ocean-continent transition (OCT) zones near the continental margins (e.g., Whitmarsh et al., 2001). In modern analogue ultra-slow spreading ocean floor, Michael et al. (2003) demonstrated the existence of a significant hydrothermal activity. These authors verified that in current Arctic Ocean (a modern analogous) the central amagmatic zone is 300 kilometres long and that the mantle peridotites are directly located on the ridge axis, similarly to what proposed for the Betic Tethys. The same authors found significant relationships between the magmatic style and rate, local tectonics and hydrothermal processes. Many Betic ophiolites outcrops appear to have suffered hydrothermal activity, testified by the occurrence of rodingitized dolerite dykes intruded in peridotites (Puga et al., 1997; 1999a; 1999b; 2002a; 2002b, 2005, 2011, 2017, Alt et al., 2012). As noted above, this indicates that ocean floor alteration/metasomatic processes scavenged CaO from ultramafic rocks and metasomatised dolerite dikes, ultimately leading to formation of rodingites (Puga et al., 1999b; 2011). The ultra-slow spreading ocean floors are also characterized by a thick cover of pelitic sediments, an issue that is also common in the Betic ophiolites, whose sedimentary sequence is exceptionally thick (around 2 km), and indistinctly covers different mantle, plutonic and volcanic sequences (Fig. 13).

According to Puga et al. (2017), the subduction of the Betic Tethys initiated in the Late Cretaceous, lasted around 30-40 Ma, and affected the whole ocean floor and part of the two continental margins located on both sides (the NW part including the Veleta Complex and the SE part including the Sabinas Unit, Figs. 14B and 14C). The eoalpine subduction of the Betic Tethys involved the mafic, ultramafic and sedimentary rocks of the ocean floor, although also part of the rocks from both margins reached metamorphic conditions in eclogite facies. The rocks of the Veleta units, far from the subduction zone, escaped the high-pressure metamorphism, and underwent the conditions of amphibolitic facies (Puga et al., 2000; 2007). The subducted Betic ophiolitic rocks reached depths between 50 km and more than 100 km (Puga et al., 1995; 1997; 1999b; 2000; 2009a; 2017; Trommsdorff et al., 1998; Ruiz-Cruz et al., 1999; Padrón-Navarta et al., 2013).

BOA geological evolution followed the eoalpine and mesoalpine re-organization of the AlKaPeCa (Alboran, Kabilias, Peloritani, Calabria) microplate (also known as Mesomediterranean microplate), which occurred in the Late Cretaceous and Paleogene, in the Early Oligocene and, especially, during Early Miocene within a compressive framework that implied plate margins deformation including the Nevado-Filábride Domain. The result of the pre-orogenic and orogenic processes in the Betic Internal Zones was the formation of a proto-chain that was rapidly dismembered into fragments dispersed in the different chains of the Western Mediterranean Alpine Orogen (Rosenbaum et al., 2002). This evolution was accompanied by the SW displacement of the Alborán block, from the Oligocene during mesoalpine metamorphic event, which ended when it reached its current position.

CONCLUSIONS

The BOA constitutes a vestige of a fragmented and metamorphosed old ocean basin opened during the Mesozoic in the Western Alpine Tethys-Mediterranean as a result of the Pangea break-up. The rifting and subsequent drifting and ocean opening were possibly influenced by pre-existing tectonic structures inherited from the Variscan orogeny. The ancient Betic Tethys originated starting from the Pliensbachian (Early Jurassic) and connected to the east with other ocean basins, currently represented by the ophiolites of the Alpine and Apennine domains, and to the west with the incipient central Atlantic Ocean. The Bétic Tethys must have been relatively narrow, with a limited width of few hundred kilometers at most. It was surely dissected by many transform faults and by extensive take-offs by low-angle faults. This result in an ocean floor composed of magmatic sectors characterized by basalts with pillow-lavas and gabbros, alternated, with amagmatic sectors, characterized by direct exposure on the ocean floor of ultramafic rocks, locally intruded by doleritic
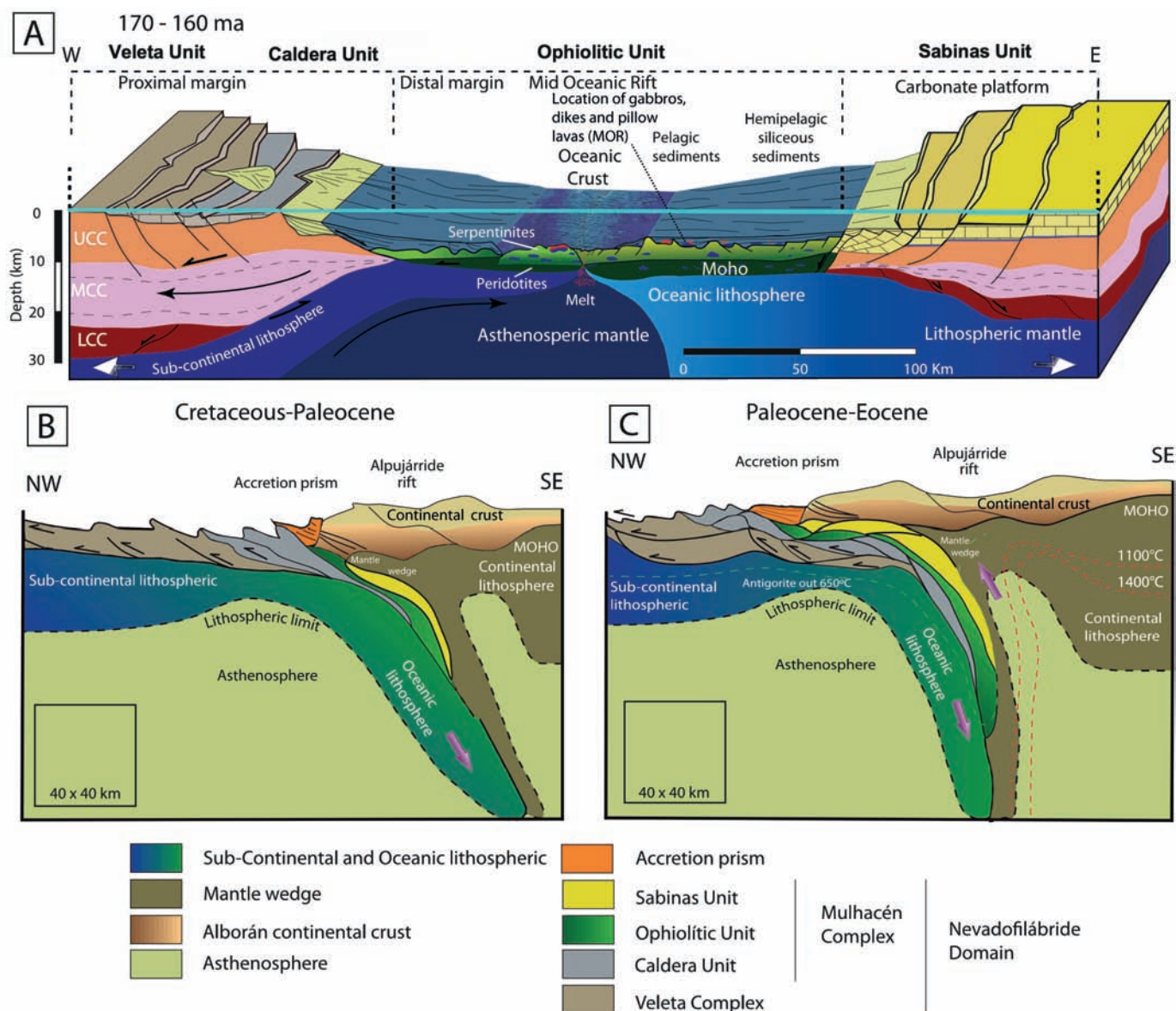
Fig. 13 - A: Paleogeographic reconstruction the Betic Tethys ocean floor during the Jurassic. Mid-oceanic accretion stage of an ultra-slow spreading ridge (< 20 mm / year), locally characterized by amagmatic sectors by high sedimentation rate. UCC: Upper Continental crust; MCC: Middle continental crust; LCC: Lower continental crust (modified from Hirth and Guillot, 2013 and Guillot et al., 2015); B and C: Geodynamic evolution of the Nevado-Filábride Domain during the Cretaceous-Paleogene convergent stage. B: Eoalpine subduction of the ocean floor and adjacent continental margins and metamorphism in eclogite facies; C: Partial exhumation of the subducted units and mesoalpine metamorphic evolution.

dikes. Similar to many Ligurian ophiolites, which are often associated with the remnants of the continental crust, BOA presents local indications of crustal assimilation, probably derived from rocks of the continental margins. This indicates a) proximity to the continental margin, at least during the early stages of ocean magmatism; and b) intermittent accretion, generally attributed to the ultra-slow spreading ridges (Puga et al., 2011). The convergence that began in the Late Cretaceous, after the reorganization of the main plates, interposed continental blocks (AlKaPeCa: Alboran, Kabilias, Peloritani, Calabria), determined the beginning of the subduction of the Betic ocean floor. This subduction was probably directed towards the S and SE, as it happened in other northern Alpine-Apennine domains and persisted until the Early Paleogene. The subducted BOA rocks were affected by an eoalpine metamorphism in the eclogite facies that ended with the exhumation of part of the studied ophiolite. This process was characterized by a pressure drop during partial exhumation of the BOA rocks and the initiation of retrograde metamorphism, which took place from the Late Paleogene, as indicated by the Ar/Ar datings on an amphibolite of Sierra de Baza (Puga et al., 2017).

REFERENCES

Aerden D.G.A.M., Bell T.H., Puga E., Sayab M., Lozano J.A. and Diaz de Federico A., 2013. Multi-stage mountain building vs. relative plate motions in the Betic Cordillera deduced from integrated microstructural and petrological analysis of porphyroblasts inclusion trails. Tectonophysics, 587: 188-206.

Aldanmaz E. and Koprubasi N., 2006. Platinum-group-element systematics of peridotites from ophiolite complexes of northwest Anatolia, Turkey: Implications for mantle metasomatism by melt percolation in a supra-subduction zone environment. Intern. Geol. Rev., 48: 420-442.

Allen D.E. and Seyfried W.E. Jr., 2003. Compositional controls on vent fluids from ultramafic-hosted hydrothermal systems at midocean ridges: An experimental study at 400°C, 500 bars. Geochim. Cosmochim. Acta, 67: 1531-1542.

Allen D.E. and Seyfried W.E., 2005. REE controls in ultramafic hosted MOR hydrothermal systems: an experimental study at elevated temperature and pressure. Geochim. Cosmochim. Acta, 69: 675-683.

Alt J.C., Garrido C.J., Shanks W.C., Turchyn A., Padròn-Navarta J.A., Lòpez-Sànchez-Vizcaino V., Gómez-Pugnaire M.T. and Marchesi C., 2012. Recycling of water, carbon, and sulfur during subduction of serpentinites: A stable isotope study of Cerro del Almirez, Spain, Earth Planet. Sci. Lett., 327/328: 50-60.

Anselmi B., Mellini M. and Viti C., 2000. Chlorine in the Elba, Monti Livornesi and Murlo serpentines: Evidence for sea-water interaction. Eur. J. Miner., 12: 137-146.

Arai S. and Ishimaru S., 2008. Insights into petrological characteristics of the lithosphere of mantle wedge beneath arcs through peridotite xenoliths: a review. J. Petrol., 49: 665-695.

Augustin N., Paulick H., Lackschewitz K.S., Eisenhauer A., Garbe-Schönberg D., Kuhn T., Botz R. and Schmidt M., 2012. Alteration at the ultramafic-hosted Logatchev hydrothermal field: Constraints from trace element and Sr-O isotope data. Geochem. Geophys. Geosyst., 13: Q0AE07. doi: 10.1029/2011GC003903.

Bach W., Garrido C.J., Paulick H., Harvey J. and Rosner M., 2004. Seawater-peridotite interactions: first insights from ODP Leg 209, MAR 15°N. Geochem., Geophys., Geosyst., 5. http://dx.doi.org/10.1029/2004GC000744.

Basch V., Rampone E., Crispini L., Ferrando C., Ildefonse B. and Godard M., 2019. Multi-stage reactive formation of troctolites in slow-spreading oceanic lithosphere (Erro-Tobbio, Italy): a combined field and petrochemical study. J. Petrol., 60: 873-906.

Bau M., 1991. Rare earth element mobility during hydrothermal and metamorphic fluid-rock interaction and the significance of the oxidation state of europium. Chem. Geol., 93: 219-230.

Bau M. and Dulski P., 1995. Comparative study of yttrium and rare-earth element behaviours in fluorine-rich hydrothermal fluids. Contrib. Miner. Petrol., 119: 213-223.

Bau, M. Dulski P. and Möller P., 1995). Yttrium and holmium in South Pacific seawater: Vertical distribution and possible fractionation mechanisms. Chem. Erde-Geochem., 55: 1-15.

Beccaluva L., Dostal J., Macciota G. and M. Zerbi, 1983. Trace element geochemistry of some ophiolites from Calabria (Southern ltaly). Ofioliti, 8: 325-332.

Beccaluva L., Ohnenstetter D. and Ohnenstetter M., 1979. Geochemical discrimination between ocean-floor and island-arc tholeiites. Appication to some ophiolites. Can. J. Earth Sci., 16: 1874-1882.

Bideau D., Hébert R., Hékinian R. and Cannat M., 1991. Metamorphism of deep-seated rocks from the Garrett Ultrafast Transform (East Pacific Rise near 13°25-S). J. Geophys. Res., 96: 10079-10099.

Bill M., Nägler Th.F. and Masson H., 2000. Major, minor, trace element, Sm-Nd and Sr isotope compositions of mafic rocks from the earliest oceanic crust of the Alpine Tethys. Schweiz. Miner. Petrogr. Mitt., 80: 131-145.

Bodinier J.L. and Godard M., 2003. Orogenic, ophiolitic, and abyssal peridotites. In: R.W. Carlson (Ed.), Treatise on Geochemistry, vol. 2., The Mantle and Core. Elsevier Sci. Ltd., p. 103-170.

Bodinier J.L., Dupuy C. and Dostal J., 1988. Geochemistry and petrogenesis of Eastern Pyrenean peridotites. Geochim. Cosmochim. Acta, 52: 2893-2907.

Bodinier J.L., Puga E., Diaz de Federico A., Leblanc M. and Morten L. 1993. Secondary harzburgites with spinifex-like textures in the Betic Ophiolitic Association (SE Spain). Terra Nova Abstr.t, 4,: 3.

Bonatti E., 1976. Serpentinite protrusions in the oceanic crust. Earth Planet. Sci. Lett., 32: 107-113.

Borghini G., Rampone E., Crispini L., De Ferrari R. and Godard M., 2007. Origin and emplacement of ultramafic-mafic intrusions in the Erro-Tobbio mantle peridotite (Ligurian Alps, Italy). Lithos, 94: 210-229.

Borghini G., Rampone E., Zanetti A., Class C., Cipriani A., Hofmann A.W. and Goldstein S., 2016. Pyroxenite layers in the Northern Apennines upper mantle (Italy) - generation by pyroxenite melting and melt infiltration. J. Petrol., 57: 625-653.

Boschi C., Bonatti E., Ligi M., Brunelli D., Cipriani A., Dallai L., D'Orazio M., Früh-Green G.L., Tonarini S., Barnes J.D. and Bedini R.M., 2013. Serpentinization of mantle peridotites along an uplifted lithospheric section, Mid Atlantic Ridge at 11° N. Lithos, 178: 3-23.

Breeding C.M., Ague J.J. and Bröcker M., 2004. Fluid-metasedimentary rock interactions and the chemical composition of arc magmas. Geology, 32: 1041-1044.

Burke W.H., Denison R.E., Hetherington E.A., Koepnick R.B., Nelson H.F. and Otto J.B., 1992. Variation of sea water 87Sr/86Sr throughout Phanerozoic time. Geology, 10: 516-519.

Cannaò E., Agostini S., Scambelluri M., Tonarini S. and Godard M., 2015. B, Sr and Pb isotope geochemistry of high-pressure Alpine metaperidotites monitors fluid-mediated element recycling during serpentinite dehydration in subduction melange (Cima di Gagnone, Swiss Central Alps). Geochim. Cosmochim. Acta, 163: 80-100.

Cannat M., 1993. Emplacement of mantle rocks in the seafloor at Mid-Atlantic Ridges. J. Geophys. Res., 98: 4163-4172.

Cannat M., Mével C., Maia M., Deplus C., Durand C., Gente P., Agrinier P., Belarouchi A., Dubuisson G., Hulmer E. and Reynolds J., 1995. Thin crust, ultramafic exposures, and rugged faulting patterns at the Mid-Atlantic Ridge (22°24'N). Geology, 23: 49-52.

Carlson R.L., 2001. The abundance of ultramafic rocks in Atlantic Ocean crust. Geophys. J. Intern., 144: 37-48.

Chalot-Prat F., Ganne J. and Lombard A., 2003. No significant element transfer from the oceanic plate to the mantle wedge during subduction and exhumation of the Tethys lithosphere (Western Alps). Lithos, 69: 69-103.

Cipriani A., Brueckner H.K., Bonatti E. and Brunelli D., 2004. Oceanic crust generated by elusive parents: Sr and Nd isotopes in basalt-peridotite pairs from the Mid-Atlantic Ridge. Geology, 32: 657-660.

Coleman R.G., 1977. Ophiolites. Springer-Verlag, New-York. 229 pp.

Deschamps F., Godard M., Guillot S., Chauvel C., Andreani M., Hattori K., Wunder B. and France L., 2012. Behavior of fluid-mobile elements in serpentines from abyssal to subduction environments: Examples from Cuba and Dominican Republic. Chem. Geol., 312/313: 93-117.

Deschamps F., Godard M., Guillot S. and Hattori K., 2013. Geochemistry of subduction zone serpentinites: A review. Lithos, 178: 96-127.

Deschamps F., Guillot S., Godard M., Andreani M. and Hattori K., 2011. Serpentinites act as sponges for fluid-mobile elements in abyssal and subduction zone environments. Terra Nova, 23: 171-178.

Deschamps F., Guillot S., Godard M., Chauvel C., Andreani M. and Hattori K., 2010. In situ characterization of serpentinites from forearc mantle wedges: timing of serpentinization and behavior of fluid-mobile elements in subduction zones. Chem. Geol., 269: 262-277.

Desmurs L., Müntener O. and Manatschal G., 2002. Onset of magmatic accretion within a magma-poor rifted margin: a case study from the Platta ocean-continent transition, eastern Switzerland. Contrib. Miner. Petrol., 144 (3): 365-382.

Dick H.J.B., Lin J. and Schouten H., 2003. An ultraslow-spreading class of ocean ridge. Nature, 426: 405-412.

Douville E., Bienvenu P., Charlou J.L., Donval J.P., Fouquet Y., Appriou P. and Gamo T., 1999. Yttrium and rare earth elements in fluids from various deep-sea hydrothermal systems. Geochim Cosmochim. Acta, 63: 627-643.

Epp D. and Suyenaga W., 1978. Thermal contraction and alteration of the oceanic crust. Geology, 6: 726-728.

Escartin J., Mével C., MacLeod C.J. and McCaig A.M., 2003. Constraints on deformation conditions and the origin of oceanic detachments: the mid-Atlantic ridge core complex at 15-45°N. Geochem. Geophys. Geosyst., 4: 1-37.

Favre P. and Stampfli G.M., 1992. From rifting to passive margin: the examples of the Red Sea, Central Atlantic and Alpine Tethys. Tectonophysics, 215: 69-97.

Floyd P.A. and Winchester J.A., 1975. Magma type and tectonic setting discrimination using immobile elements. Earth Planet. Sci. Lett., 27: 211-218.

Francis T.J.G., 1981. Serpentinization faults and their role in the tectonics of slow spreading ridges. J. Geophys. Res., 86: 11616-11622.

Gale A., Dalton C.A., Langmuir C.H., Su Y. and Schilling J.G., 2013. The mean composition of ocean ridge basalts. Geochem. Geophys. Geosyst., 14: 489-518.

Garrido C.J., López Sánchez-Vizcaíno V., Gómez-Pugnaire M.T., Trommsdorff V., Alard O., Bodinier J.L. and Godard M., 2005. Enrichment of HFSE in chlorite-harzburgite produced by high-pressure dehydration of antigorite-serpentinite: Implications for subduction magmatism. Geochem. Geophys. Geosyst., 6: Q01J15.

Gómez-Pugnaire M.T., Braga J.C., Martín J.M., Sassi F.P. and Moro A., 2000. Regional implications of a Palaeozoic age for the Nevado-Filabride cover of the Betic Cordillera, Spain. Schweiz. Miner. Petrogr. Mitt., 80: 45-52.

Govindaraju K., 1994. Compilation of working values and sample description for 383 geostandards. Geostand. Newsl., 18: 1-158.

Guerrera F., Martin-Algarra F. and Perrone V., 1993. Late Oligocene-Miocene syn-late orogenic successions in western and central Mediterranean chains from the Betic Cordillera to the Southern Apennines. Terra Nova, 5: 525-544.

Guillot S., Schwartz S., Reynard B., Agard P. and Prigent C., 2015. Tectonic significance of serpentinites. Tectonophysics, 646: 1-19.

Haas J.R., Shock E.L. and Sassani D.C., 1995. Rare earth elements in hydrothermal systems: Estimates of standard partial molal thermodynamic properties of aqueous complexes of the rare earth elements at high pressures and temperatures. Geochim. Cosmochim. Acta, 59 (21): 4329-4350.

Handy M.R., Schmid S.M., Bousquet R., Kissling E. and Bernoulli D., 2010. Reconciling plate-tectonic reconstructions of Alpine Tethys with the geological-geophysical record of spreading and subduction in the Alps. Earth Sci. Rev., 102: 121-158.

Hart S.R. and Zindler A., 1986. In search of a bulk-Earth composition. Chem. Geol., 57: 247-267.

Herbrich A., Hoernle K., Werner R., Hauff F., van den Bogaard P. and Garbe-Schönberg D., 2015. Cocos Plate Seamounts offshore NW Costa Rica and SW Nicaragua: Implications for large-scale distribution of Galápagos plume material in the upper mantle. Lithos, 212/215: 214-230.

Hirth G. and Guillot S., 2013. Rheology and tectonic significance of serpentinite. Elements, 9: 107-113.

Hoffman A.V., 1997. Mantle geochemistry: the message from oceanic volcanism. Nature, 385: 219-229.

Irvine T.N. and Baragar W.R.A., 1971. A guide to the chemical classification of the common volcanic rocks. Can. J. Earth Sci., 8: 523-548.

Jagoutz E., Palme H., Baddenhausen H., Blum K., Cendales M., Dreibus G., Spettel B., Lorenz V. and Vanke H., 1979. The abundance of major, minor and trace elements in the earth's mantle as derived from primitive ultramafic nodules. Geochim. Cosmochim. Acta, 11 (2): 2031-2050.

Janecky D.R. and Seyfried W.E. Jr., 1986. Hydrothermal serpentinization of peridotite within the oceanic crust: experimental investigations of mineralogy and major element chemistry. Geochim. Cosmochim. Acta, 50: 1357-1378.

John T., Scambelluri M., Frische M., Barnes J. and Bach W., 2011. Dehydration of subducting serpentinite: implications for halogen mobility in subduction zones and the deep halogen cycle. Earth Planet. Sci. Lett., 308: 65-76.

Jones C.E., Jenkyns H.C., Coe A.L. and Hesselbo S.P., 1994. Strontium isotopic variations in Jurassic and Cretaceous sea water. Geochim. Cosmochim. Acta, 58: 3061-3074.

Jöns N., Bach W. and Klein F., 2010. Magmatic influence on reaction paths and element transport during videnceization. Chem. Geol., 274: 196-211.

Karson J.A. and Lawrence R.M., 1997. Tectonic setting of serpentinite exposures on the western median valley wall of the MARK area in the vicinity of site 920. In: J.A Karson, M. Cannat, D.J. Miller and D. Elthon (Eds.), Proceed. O.D.P., Sci. Res., 153: 5-21.

Karson J.A., Kelley D.S., Williams E.A., Yoerger D.R. and Jakuba M., 2006. Detachment shear zone of the Atlantis Massif core complex, Mid-Atlantic Ridge, 30°N. Geochem. Geophys. Geosyst., 7: Q06016.

Kendrick M.A., Scambelluri M., Honda M. and Phillips D., 2011. High abundances of noble gas and chlorine delivered to the mantle by serpentinite subduction. Nature Geosci., 4: 807-812.

Kodolányi J., Pettke T., Spandler C., Kamber B.S. and Gméling K., 2012. Geochemistry of ocean floor and fore-arc serpentinites: constraints on the ultramafic input to subduction zones. J. Petrol., 53: 235-270.

Kretz R. 1983. Symbols of rock-forming minerals. Am. Miner., 68: 277-279.

Lafay R., Deschamps F., Schwartz S., Guillot S., Godard M., Debret B. and Nicollet C., 2013. High-pressure serpentinites, a trap-and-release system controlled by metamorphic conditions: example from the Piedmont zone of the western Alps. Chem. Geol., 343: 38-54.

Lagabrielle Y., 2009. Mantle exhumation and lithospheric spreading: An historical perspective from investigations in the oceans and in the Alps-Appennines ophiolites. It. J. Geosci., 12: 279-293.

Lagabrielle Y., Vitale Bovarone A. and Ildefonse B., 2015. Fossil oceanic core complexes recognized in the blueschist metaophiolites of Western Alps and Corsica. Earth-Sci. Rev., 141: 1-26.

Le Bas M.J. and Streckeisen A.L., 1991. The IUGS systematics of igneous rocks. J. Geol. Soc. London, 148: 825-833.

Li Y.H. and Schoonmaker J., 2003. Chemical composition and mineralogy of marine sediments. In: F.T. Mackenzie (Ed.), Sediments, diagenesis, and sedimentary rocks, Treatise on geochemistry. Elsevier Sci. Ltd., 7: 1-35.

López Sánchez-Vizcaíno V., Trommsdorff V., Gómez-Pugnaire M.T., Garrido C.J., Müntener O. and Connolly J.A.D., 2005. Petrology of titanian clinohumite and olivine at the high-pressure breakdown of antigorite serpentinite to chlorite harzburgite (Almirez Massif, S. Spain). Contrib. Miner. Petrol., 149: 627-646.

Lozano J.A., Puga E., Garcia-Casco A., Martínez-Sevilla F., Contreras Cortés F., Carrasco Rus J. and Martín-Algarra A., 2018. First evidence of prehistoric eclogite quarrying for polished tools and their circulation on the Iberian Peninsula. Geoarchaeol., 33: 364-385.

MacLeod C., Searle R.C., Murton B.J., Casey J.F., Mallows C., Uns worth S.C., Achenbach K.L. and Harris M., 2009. Life cycle of oceanic core complexes. Earth Planet. Sci. Lett., 287: 333-344.

Manatschal G. and Müntener O., 2009. A type sequence across an ancient magma- poor ocean-continent transition: the example of the western Alpine Tethys ophiolites. Tectonophysics, 473: 4-19.

Marchesi C., Garrido C.J., Godard M., Belley F. and Ferré E., 2009. Migration and accumulation of ultra-depleted subduction-related melts in the Massif du Sud ophiolite (New Caledonia). Chem. Geol., 266: 171-186.

Marchesi C., Garrido C.J., Godard M., Proenza J.A., Gervilla F. and Blanco-Moreno J., 2006. Petrogenesis of highly depleted peridotites and gabbroic rocks from the Mayari-Baracoa Ophiolitic Belt (eastern Cuba). Contrib. Miner. Petrol., 151: 717-736.

Marchesi C., Garrido C.J., Padrón-Navarta J.A., López Sánchez-Vizcaíno V. and Gómez-Pugnaire M.T., 2013. Element mobility from seafloor serpentinization to high-pressure dehydration of antigorite in subducted serpentinite: Insights from the Cerro del Almirez ultramafic massif (southern Spain). Lithos, 178: 128-142.

Marroni M., Molli G., Montanini A. and Tribuzio R., 1998. The association of continental crust rocks with ophiolites (Northern Apennines, Italy): Implications for the continent-ocean transition. Tectonophysics, 292: 43-66.

Marzoli A., Renne P.R., Piccirillo E.M., Ernesto M., Bellieni G. and De Min A., 1999. Extensive 200-Million-year-old continental flood basalts of the Central Atlantic Magmatic Province. Science, 284: 616-618.

McDonough W.F. and Sun S.-S. 1995. The composition of the Earth. Chem. Geol., 120: 223-253.

Menzies M.A., Long A., Ingram G., Tatnell M. and Janecky D., 1993. MORB peridotite-sea water interaction: experimental constraints on the vidence of trace elements, $^{87}Sr/^{86}Sr$ and $^{143}Nd/^{144}Nd$ ratios. In: H.M. Prichard, T. Alabaster, N.B.W. Harris and C.R. Neary (Eds.), Magmatic processes and plate tectonics. Geol. Soc. London Spec. Publ., 76: 309-322.

Mével C., 2003. Serpentinization of abyssal peridotites at mid-ocean ridges. C.R. Géosci., 335: 825-852.

Michael P.J., Langmuir C.H., Dick H.J.B., Snow J.E., Goldstein S.L., Graham D.W., Lehnert K., Kurras G., Jokat W., Mühe R. and Edmonds H.N., 2003. Magmatic and amagmatic seafloor generation at the ultraslow-spreading Gakkel ridge, Arctic Ocean. Nature, 423: 956-961.

Miyashiro A., 1975. Classification, characteristics and origin of ophiolites. J. Geol., 83: 249-281.

Miyashiro A., Shido F. and Ewing M., 1969. Composition and origin of serpentinites from the Mid-Atlantic Ridge near 24 and 30°N. Contrib. Miner. Petrol., 23: 117-127.

Montanini A., Tribuzio R. and Vernia L., 2008. Petrogenesis of basalts and gabbros from an ancient continent-ocean transition (External Liguride ophiolites, Northern Italy). Lithos, 101: 453-479.

Morishita T., Hara K., Nakamura K., SawaguchiT., Tamura A., Arai S., Okino K., Takai K. and Kumagai H., 2009. Igneous, alteration and exhumation processes recorded in abyssal peridotites and related fault rocks from an oceanic core complex along the Central Indian Ridge. J. Petrol., 50: 1299-1325.

Morten L., Bargossi G.M., Martınez-Martınez J.M., Puga E. and Dıaz de Federico A., 1987. Meta-gabbro and associated eclogites in the Lubrın area, Nevado-Filabride complex, Spain, J. Metam. Geol., 5: 155-174.

Nieto J.M., 1996. Petrología y geoquímica de los or togneises del Complejo del Mulhacén, Cordilleras Béticas. Ph. D. Thesis, Univ. Granada, 211 pp.

Nieto J.M., Puga E. and Díaz De Federico A., 2000. Late Variscan pyroclastic rocks from the Mulhacén Complex (Betic Cordillera, Spain). In: H. Leyrit and Ch. Montenat (Eds), Volcaniclastic rocks, from magmas to sediments. Gordon and Breach Sci. Publ., p. 217-224.

Niu Y., 2004. Bulk-rock major and trace element compositions of abyssal peridotites: implications for mantle melting, melt extraction and post-melting processes beneath mid-ocean ridges. J. Petrol., 45: 2423-2458.

Niu Y., Langmuir C.H. and Kinzler R.J., 1997. The origin of abyssal peridotites: a new perspective. Earth Planet. Sci. Lett., 152: 251-265.

O'Hanley D.S., 1991. Fault-related phenomena associated with hydration and serpentine recrystallization during serpentinization. Can. Miner., 29: 21-35.

Olivier N. and Boyet M., 2006. Rare earth and trace elements of microbialites in Upper Jurassic coral- and sponge-microbialite reefs. Chem. Geol., 230: 105-123.

Padrón-Navarta J.A., López Sanchez-Vizcaino V., Hermann J., Connolly J.A.D., Garrido C.J., Gómez-Pugnaire M.T. and Marchesi C., 2013. Tschermak's substitution in antigorite and consequences for phase relations and water liberation in high-grade serpentinites. Lithos, 178: 186-196.

Palandri J.L. and Reed M.H., 2004. Geochemical models of metasomatism in ultramafic systems: serpentinization, rodingitization, and sea floor carbonate chimney precipitation. Geochim. Cosmochim. Acta, 68: 1115-1133.

Parkinson I.J. and Pearce J.A., 1998. Peridotites from the Izu-Bonin-Mariana forearc (ODP Leg 125): Evidence for mantle melting and melt-mantle interaction in a supra-subduction zone setting. J. Petrol., 39: 1577-1618.

Paulick H., Bach W., Godard M., De Hoog J.C.M., Suhr G. and Harvey J., 2006. Geochemistry of abyssal peridotites (Mid-Atlantic Ridge, 15°20-N, ODP Leg 209): implications for fluid/rock interaction in slow spreading environments. Chem. Geol., 234: 179-210.

Pearce J.A., 1982. Trace element characteristics of lavas from destructive plate boundaries. In: R.S. Thorpe (Ed.), Orogenic andesites and related rocks. John Wiley and Sons, Chichester, England, p. 528-548.

Pearce J.A., 1996. A user's guide to basalt discrimination diagrams. In: D.A. Wyman (Ed.), Trace element geochemistry of volcanic rocks: Applications for massive sulphide exploration. Short Course Notes. Geol. Ass. Can., 12: 79-113.

Pearce, J.A., 2003. Supra-subduction zone ophiolites: The search for modern analogues. In: Y. Dilek and S. Newcomb (Eds.), Ophiolite concept and the evolution of geological trhought. Geol. Soc. Am. Spec. Pap., 373: 269-293.

Pearce J.A., 2008. Geochemical fingerprinting of oceanic basalts with applications to ophiolite classification and the search of the Archean oceanic crust. Lithos, 100: 14-48.

Pearce J.A. and Peate D.W.,1995. Tectonic implications of the composition of volcanic arc magmas. Ann. Rev. Earth Planet. Sci., 23: 251-285, doi: 10.1146/annurev.ea.23.050195.001343

Pearce J.A., Barker P.F., Edwards S.J., Parkinson I.J. and Leat P.T., 2000. Geochemistry and tectonic significance of peridotites from the South Sandwich arc-basin system, South Atlantic. Contrib. Miner. Petrol., 139: 36-53.

Pearce J.A., Harris N.B.W. and Tindle A.G., 1984. Trace element cliscrimination diagrams for the tectonic interpretation of granitic rocks. J. Petrol., 25: 956-983.

Piccardo G.B. and Guarnieri L., 2010. Alpine peridotites from the Ligurian Tethys: an updated critical review. International Geol. Rev., 52: 1138-1159.

Plank T. and Langmuir C.H., 1998. The chemical composition of subducting sediments and its consequences for the crust and mantle. Chem. Geol., 145: 325-394.

Puga E., 1977. Sur l'existence dans le complexe de la Sierra Nevada (Cordillère Bétique, Espagne du sud) d'éclogites et sur leur origine probable à partir d'une croûte océanique mésozoique. C.R. Acad. Sci., 285: 1379-1382. (In French)

Puga E., 1990. The Betic Ophiolitic Association (Southeastern Spain). Ofioliti, 15: 97-117.

Puga E., 2005. A reappraisal of the Betic Ophiolitic Association: The westernmost relic of the Alpine Tethys Ocean. In: I.R. Finetti (Ed.), Deep seismic exploration of the Central Mediterranean and Italy. CROP 1 Volume, Univ. Trieste, Italy, Elsevier, p. 665-704.

Puga E. and Díaz de Federico A., 1978. Metamorfismo polifásico y deformaciones alpinas en el Complejo de Sierra Nevada (Cordillera Bética). Implicaciones geodinámicas. In: Reunión sobre la geodinámica de las Cordilleras Béticas y el Mar de Alborán. Univ. Granada, Secret. Publ., Granada, Spain, p. 79-111 (In Spanish).

Puga E., Bodinier J.L., Díaz de Federico A., Morten L. and Nieto J.M., 1997. Pseudo-spinifex meta-ultramafic rocks containing eclogitized rodingite dykes in the Betic Ophiolitic Association (SE Spain): evidence of Alpine subduction following an ocean-floor metasomatic process. Quad. Geodin. Alp. Quatern., 4: 98-99.

Puga E., Díaz de Federico A., Bargossi G.M. and Morten L., 1989a. The Nevado-Filábride metaophiolitic association in the Cóbdar region (Betic Cordillera, SE Spain): preservation of pillow structures and development of coronitic eclogites. Geodin. Acta, 3: 17-36.

Puga E., Díaz De Federico A. and Demant A., 1995. The eclogitized pillows of the Betic Ophiolitic Association: Relics of the Tethys ocean floor incorporated to the Alpine Chain after subduction. Terra Nova, 7: 32-43.

Puga E., Díaz de Federico A., Fediukova E., Bondi M. and Morten L., 1989b. Petrology, geochemistry and metamorphic evolution of the ophiolitic eclogites and related rocks from the Sierra Nevada (Betic Cordilleras, southeastern Spain). Schweiz. Miner. Petrogr. Mitt., 69: 435-455.

Puga E., Díaz De Federico A., Manteca Martinez J.I., Rodríguez Martinez Conde J.A. and Díaz Puga M.A., 2004a. The Canteras-Galifa Neogene conglomerates: Evidence for an ophiolitic association submerged in the Mediterranean Sea at the eastern end of the Betic Chain. Ofioliti, 29: 213-230.

Puga E., Díaz de Federico A., Fanning M., Nieto J.M., Rodríguez Martínez-Conde J.A., Díaz Puga M.A., Lozano J.A., Bianchini G., Natali C. and Beccaluva L. 2017. The Betic ophiolites and the evolution of the western Tethys. Geosciences, 7: 31.

Puga E., Díaz de Federico A. and Nieto J.M. 2002a. Tectonostratigraphic subdivision and petrological characterisation of the deepest complexes of the Betic zone: a review. Geodin. Acta, 15: 23-43.

Puga E., Díaz de Federico A., Nieto J.M. and Díaz Puga M.A., 2007. Petrología, evolución geodinámica y georrecursos del Espacio Natural de Sierra Nevada. Estud. Geol., 6: 19-40.

Puga E., Díaz de Federico A., Nieto J.M., Díaz Puga M.A. and Rodríguez Martínez-Conde J.A., 2009. The Betic Ophiolitic Association: A very significant geological heritage that needs to be preserved. Geoheritage, 1: 11-31.

Puga E., Díaz De Federico A., Nieto J.M., Díaz Puga M.A., Rodríguez Martinez Conde J.A. and Manteca Martinez J.I., 2004b. Argumentos petro- lógicos y geoquímicas para la subdivisión del Complejo Nevado-Filábride en los Complejos del Veleta y del Mulhacén. VI Congr. Geol. España, Zaragoza (España). Geo-Temas, 6: 101-104.

Puga E., Fanning C.M., Díaz de Federico A., Nieto J.M., Beccaluva L., Bianchini G. and Díaz Puga M.A., 2011. Petrology, geochemistry and U-Pb geochronology of the Betic Ophiolites: Inferences for Pangaea break-up and birth of the westernmost Tethys Ocean. Lithos, 124: 255-272.

Puga E., Fanning C.M., Nieto J.M. and Díaz de Federico A., 2005. New recrystallization textures in zircons generated by ocean-floor and eclogite facies metamorphism: a cathodoluminescence and U-Pb SHRIMP study with constraints from REE elements. Can. Miner., 42: 183-202.

Puga E., Nieto J.M. and Díaz de Federico A., 2000. Contrasting P-T paths in eclogites of the Betic Ophiolitic Association (Mulhacén Complex, SE Spain). Can. Miner., 38: 1137-1161.

Puga E., Nieto J.M., Díaz de Federico A., Bodinier J.L. and Morten L., 1999a. Petrology and metamorphic evolution of ultramafic rocks and dolerite dykes of the Betic Ophiolitic Association (Mulhacén Complex, SE Spain): evidence of Eo-Alpine subduction following an ocean-floor metasomatic process. Lithos, 49: 107-140.

Puga E., Ruiz Cruz M.D. and Díaz De Federico A., 1999b. Magnetite-silicate inclusions in olivine of ophiolitic meta-gabbros from the Mulhacén Complex (Betic Cordillera, SE Spain). Can. Miner., 37: 1191-1209.

Puga E., Ruiz Cruz M.D. and Díaz De Federico A., 2002b. Polymetamorphic amphibole veins in metabasalts from the Betic Ophiolitic Association (SE Spain): Relics of ocean-floor metamorphism preserved throughout the Alpine Orogeny. Can. Miner., 40: 67-83.

Rampone E. and Hofmann A.W., 2012. A global overview of isotopic heterogeneities in the oceanic mantle. Lithos, 148: 247-261.

Rampone E. and Piccardo G.B., 2000. The ophiolite-oceanic lithosphere analogue: new insights from the Northern Apennine (Italy). In: J. Dilek, E. Moores, D. Elthon and A. Nicolas (Eds.), Ophiolites and oceanic crust: New insights from field studies and Ocean Drilling Program. Geol. Soc. Am. Spec. Pap., 349: 21-34.

Rampone E., Borghini G. and Basch V., 2018. Melt migration and melt-rock reaction in the Alpine-Apennine peridotites: Insights on mantle dynamics in extending lithosphere. Geosci. Front., 11: 151-166.

Rampone E., Borghini G., Romairone A., Abouchami W., Class C., and Goldstein M.L., 2014. Sm-Nd geochronology of the Erro-Tobbio gabbros (Ligurian Alps, Italy): insights into the evolution of the Alpine Tethys. Lithos, 205: 236-246.

Rampone E., Hofmann A.W., Piccardo G.B., Vannucci R., Bottazzi P. and Ottolini L., 1995. Petrology, mineral and isotope geochemistry of the External Liguride peridotites (Northern Apennines, Italy). J. Petrol., 36: 81-105.

Rampone E., Hofmann A.W and Raczek I., 1998. Isotopic constraints within the Internal Liguride ophiolite (N. Italy): the lack of a genetic mantle-crust link. Earth Planet. Sci. Lett., 16: 175-189.

Rampone E., Hofmann A.W and Raczek I., 2009. Isotopic equilibrium between mantle peridotite and melt: Evidence from the Corsica ophiolite. Earth Planet. Sci. Lett., 288: 601-610.

Rampone E., Piccardo G.B. and Hofmann A.W., 2008. E., Multistage melt-rock interaction in the Mt. Maggiore (Corsica, France) ophiolitic peridotites: microstructural and geochemical evidence. Contrib. Miner. Petrol., 156: 453-475.

Rampone E., Romairone A., Abouchami W., Piccardo G.B. and and Hofmann A.W., 2005. Chronology, petrology, and isotope geochemistry of the Erro-Tobbio peridotites (Ligurian Alps, Italy): Records of late Palaeozoic lithospheric extension. J. Petrol., 46, 799-827.

Regelous M., Weinzierl C.G. and Haase K.M., 2016. Controls on melting at spreading ridges from correlated abyssal peridotite-mid-ocean ridge basalt composition. Earth Planet, Sci. Lett., 449: 1-11.

Rosenbaum G., Lister G.S. and Duboz C., 2002. Relative motions of Africa, Iberia and Europe during Alpine orogeny. Tectonophysics, 359: 117-129.

Ruiz Cruz M.D., Puga E. and Díaz de Federico A., 2007. Exsolution microstructures in amphiboles from metabasalts of the Betic ophiolitic association (SE Spain). Eur. J. Miner., 19: 547-556.

Ruiz Cruz M.D., Puga E. and Nieto J.M., 1999. Silicate and oxide exsolution in pseudo-spinifex olivine from metaultramafic rocks of the Betic Ophiolitic Association: A TEM study. Am. Miner., 84: 1915-1924.

Saccani E., 2015. A new method of discriminating different types of post-Archean ophiolitic basalts and their tectonic significance using Th-Nb and Ce-Dy-Yb systematics. Geosci. Front., 6: 481-501.

Saccani E., Principi G., Garfagnoli F. and Menna F. 2008. Corsica ophiolites: Geochemistry and petrogenesis of basaltic and metabasaltic rocks. Ofioliti, 33: 187-207.

Salters V.J.M. and Stracke A. 2004. Composition of the depleted mantle. Geochem. Geophys. Geosyst., 5: Q05B07.

Savov I.P., Ryan J.G., D'Antonio M., Kelley K. and Mattie P., 2005. Geochemistry of serpentinized peridotites from the Mariana Forearc Conical Seamount, ODP Leg 125: Implications for the elemental recycling at subduction zones. Geochem. Geophys. Geosyst., 6: Q04J15. doi: 10.1029/2004GC000777.

Scambelluri M., Cannaò E., and Gilio M., 2019. The water and fluid-mobile element cycles during serpentinite subduction. A review. Eur. J. Miner., 31: 405-428.

Scambelluri M., Fiebig J., Malaspina N., Müntener O. and Pettke T., 2004. Serpentinite subduction: implications for fluid processes and trace-element recycling. Intern. Geol. Rev., 46: 595-613.

Schaltegger U., Desmurs L., Manatschal G., Müntener O., Meier M., Frank M. and Bernoulli D., 2002. The transition from rifting to sea-floor spreading within a magma-poor rifted margin: field and isotopic constraints. Terra Nova, 14: 156-162.

Schettino A. and Turco E., 2009. Breakup of Pangaea and plate kinematics of the Central Atlantic and Atlas regions. Geophys. J. Intern., 178: 1078-1097.

Secchiari A., Montanini A., Bosh D., Macera P. and Cluzel D., 2016. Melt extraction and enrichment processes in the New Caledonia lherzolites: evidence from geochemical and Sr-Nd isotope data. Lithos, 260: 28-43.

Secchiari A., Montanini A., Bosh D., Macera P. and and Cluzel D., 2019. Sr, Nd, Pb and trace element systematics of the New Caledonia harzburgites: Tracking source depletion and contamination processes in a SSZ setting. Geosci. Front., 11: 37-55.

Seifert K. and Brunotte D., 1996. Geochemistry of serpentinized mantle peridotite from site 897 in the Iberia Abyssal Plain. In: R.B. Whitmarsh, D.S. Sawyer, A. Klaus and D.G. Masson (Eds.), Proceed. ODP Sci. Rep., 149: 413-424.

Shervais J.N., 1982. Ti-Y plots and the petrogenesis of modern and ophiolitic lavas. Earth Planet. Sci. Lett., 59: 101-118.

Sinton J.M. and Detrick R.S., 1992. Mid-ocean ridge magma chambers. J. Geophys. Res., 97: 197-216.

Snow J.E. and Dick H.J.B., 1995. Pervasive magnesium loss by marine weathering of peridotite. Geochim. Cosmochim. Acta, 59: 4219-4235.

Snow J.E., Hart S.R. and Dick H.J.B., 1994. Nd and Sr isotope evidence linking mid-oceanridge basalts and abyssal peridotites. Nature, 371: 57-60.

Stille P., Clauer N. and Albrecht J., 1989. Nd isotope composition of the Jurassic Tethys seawater and the genesis of Alpine Mn-deposits. Evidences from Sr-Nd isotope data. Geochim. Cosmochim. Acta, 53: 1095-1099.

Sun S.S. and McDonough W.F., 1989. Chemical and isotopic systematic of oceanic basalts; implications for mantle composition and processes. In: A.D. Saunders and M.J. Norry (Eds.), Magmatism in the oceanic basins. Geol. Soc. London Spec. Publ., 4: 313-345.

Tendero J.A., Martín-Algarra A., Puga, E. and Díaz de Federico A., 1993. Lithostratigraphie des métasédiments de l'association ophiolitique Nevado-Filabride (SE Espagne) et mise en evidence d'objets ankeritiques evoquant des foraminifères planctoniques du Crétacé: consequences paléogéographiques. C.R. Acad. Sci. Paris, 316: 1115-1122.

Trommsdorff V., López Sánchez-Vizcaíno V., Gómez-Pugnaire M.T. and Müntener O., 1998. High pressure breakdown of antigorite to spinifex-textured olivine and orthopyroxene, SE Spain. Contrib. Miner. Petrol., 132: 139-148.

Ulrich M., Picard C., Guillot S., Chauvel C., Cluzel D. and Meffre S., 2010. Multiple melting stages and refertilization as indicators for ridge to subduction formation: The New Caledonia ophiolite. Lithos, 115: 223-236.

Venturelli G., Capedri S., Thorpe R.S. and Potts P.J., 1979. Rareearth and other element distribution in some ophiolitic metabasalts of Corsica, Western Mediterranean. Chem. Geol., 24: 339-353.

Wood D.A., Tarney J., Varet J., Saunders A.D., Bougault H., Joron J.L., Treuil M. and Cann J.R., 1979. Geochemistry of basalts drilled in the North Atlantic by IPOD Leg 49: implications for mantle heterogeneity. Earth Planet. Sci. Lett., 42: 77-97.

Whitmarsh R.B., Manatschal G. and Minshull T., 2001. Evolution of magma-poor continental margins from rifting to seafloor spreading. Nature, 413: 150-154.

Zheng Y.F. 2012. Metamorphic chemical geodynamics in continental subduction zones. Chem. Geol., 328: 5-48.